Solid bonding criteria design for aluminum chips recycling through Friction Stir Consolidation

R. Puleo[1], A. Latif [1], G. Ingarao[1], R. Di Lorenzo[1], L. Fratini[1]*

[1] Department of Engineering, University of Palermo, Viale delle Scienze, Palermo, 90128, Italy

**corresponding author,*

ABSTRACT

Decoupling economic growth from resource depletion is an urgent target to achieve. Adopting circular economy paradigm is the only way to address such challenge. Manufacturing scientists have to make a research effort addressed to find and design proper manufacturing processes enabling circular economy strategies such as remanufacturing, repairs, recycling, etc. This paper aims at enhancing the knowledge concerning Friction Stir Consolidation (FSC) process, a solid state innovative and resource efficient aluminum alloys scrap recycling process that directly turns a batch of chips into a consolidated billet. In this paper, FSC process is used to recycle AA7075 chips and different solid bonding criteria, already presented in literature, have been tested through an experimental and numerical approach. All of them failed to predict the chips solid bonding in FSC processes. Therefore, a new criterion, specifically designed for FSC, is presented. The performance of conventional criteria has been compared to that provided by the new criterion on two validation tests. For the analysis of the bonding prediction performance, an innovative procedure is proposed for the threshold values identification. The proposed approach is based on experimental data collection, numerical simulations and an optimization procedure implemented in MATLAB environment. The new, and here presented criterion, provided the best results with at least 90% of prediction accuracy compared to the conventional Plata – Piwnik criterion characterized by an average accuracy equal to 55%, instead. The proposed procedure, and the new identified solid bonding criterion, represent a powerful tool for understanding and designing aluminum alloys recycling through FSC.

Keywords: Friction Stir Consolidation, Solid bonding criteria, aluminum alloys, chips recycling, F.E.M

Nomenclature

FSC	Friction Stir Consolidation
Exp ID	Experimental identification number
p	Normal contact pressure
σ_{mean}	Mean stress
σ_f	Flow stress of the material
σ_b	Absolute bond strength
$\bar{\varepsilon}$	Equivalent strain
$\dot{\varepsilon}$	Strain rate
$\dot{\varepsilon}_0$	Reference strain rate

v	Nodal velocity
w_T	Temperature weight
w_s	Strain weight
Z	Zener – Hollomon parameter
W_{Ci}^{lim}	Threshold limit value for the i-th criterion
r	Correlation value
Gz	Grain size
HV	Vickers hardness value
T_i	Temperature calculated for the i-th calculation step
ε_i	Strain calculated for the i-th calculation step
t_0	Starting processing time
t_f	Final processing time

1. Introduction

Industrial activity in 2021 was directly responsible for emitting 9.4 Gt of CO_2, accounting for a quarter of global emission. The trend has been increasing as industrial emissions have risen by more than 70% since 2000 as a result of increasing global demand for industrial goods coupled with more modest increases in energy efficiency. Metals production plays a significant role in industrial direct emissions: iron and steel production accounted for 30% while aluminum production industry was responsible for about 3% of the world's CO_2 emissions in 2021. Decoupling material demand from economic and population growth can help curb CO_2 emissions from material production. The main approach for reducing the materials primary production and decoupling the resource depletion from the economic growth is the implementation of circular economy strategies. Longer life, repair, product upgrades, modularity, remanufacturing, component reuse and recycling are some of the strategies to put in place to reduce the environmental impact of raw material production (Tolio et al., 2017). As far as metals are regarded, recycling is still the most used circular economy strategy; for aluminum alloys conventional recycling allows an energy demand reduction by up to 90% for the production of 1 kilogram of usable material (Ashby, 2021). Nevertheless, for aluminum alloys the conventional recycling route, based on remelting, is still neither energy nor resource efficient. As a matter of fact, the main drawback for the conventional recycling processes is the permanent material losses occurring during remelting because of the oxidation (Douflou et al., 2015). In order to address such issue, researchers have turned to Solid State Recycling (SSR) strategies. These approaches directly turn aluminum scraps into semi-finished products by avoiding the remelting step. Solid state activation depends on pressure, temperature and contact time among surfaces to be joined. Thus, various solid state recycling techniques have been proposed based on the physical disruption and dispersion of the oxide contaminants by imposing high tempaertures, significant plastic and shear strains. Plastic deformation should be large enough to break the surface oxide layer of the metal in order to expose clean, non-oxidized metal surfaces and to allow the formation of metallic bonds. Most of the SSR approaches are based on extrusion mechanics; some authors applied high extrusion ratio direct hot extrusion (Tekkaya et al., 2009), in this research an increased level of introduced plastic strain led to the obtainement of recycled profiles with comparable mechanical properties as the cast-based ones (Chiba et al., 2014). Other authors applied a processes chain to directly obtain finished or

semi-finished products ot of chips: Chiba et al. (2011) applied a cold rolling process after the extrusion step, while Haase and Tekkaya (2015) applied a combination of hot and cold extrusion processes. A variant of this approach envisages the use and extrusion based with Equal Channel Angular Pressing (ECAP): Haase et al. (2012) obtained superior mechanical properties in the aluminum alloys recycled samples, Liu et al. (2016) applied ECAP extrusion to consolidate Ti-6Al-4V machining chips. Other authors applied screw extrusion (Widerøe and Welo, 2012) for recycling chips, in this approach the rotational movement generates extrusion pressure and introduces large shear strains that enhances the consolidation process. In this respect, some authors have recently proposed the Shear Assisted Processing and Extrusion (ShAPE) to directly turn chips into hollow extruded profiles (Whalen et al., 2023).

Other solid state recycling processes rely more on sintering phenomenon to obtain bonding conditions, the main approach is based on heating up the metallic scraps and applying vertical load to consolidate chips into billets. In this domain, Spark Plasma Sintering (SPS) has been successfully applied to recycle both aluminum (Paraskevas et al., 2014) and magnesium alloys (Paraskevas et al., 2016) chips. Li et al. (2020) improved ultimate compression stregnth and compression failture strain during SPS of magnesium alloy. Ciclo et al. (2020) applied Pulsed Electric Current Sintering (PECS) to consolidate AA6082 machining chips. However, due to the lack of strain and strain rate occurrence, the consolidation level and final density provided by this process category could not be satisfactory; for these reasons some authors proposed to add a further process step after sintering step. Kohck et al. (2020) proposed a recycling process made of a field-assisted sintering (FAST) process to consolidate the aluminum alloys chips, and a forward rod extrusion process. Behrens et al. (2014) recommended a hybrid approach made of compacting, sintering and forming to consolidate aluminum chips; Pei et al. (2022) applied an isothermal sintering process with multiple ECAP passes to increase the mechanical properties of magnesium alloys.

Other SSR approaches use the friction between a rotating tool and the chips to be recycled to produce heat and plastic deformation and achieve solid bonding conditions. One of these processes is the Friction Stir Extrusion (FSE), first presented by Tang and Reynold (2010), in this process the aluminum chips batch is consolidated into wires/rods by means of backward extrusion process. Also, FSE approach has been successfully applied to turn magnesium chips into wires (Baffari et al., 2017).

The other SSR process belonging to the friction based category is the Friction Stir Consolidation (FSC), this process effectively turns machining chips directly into solid blocks/billets (Li et al., 2018). Actually, a rotating tool is pressed onto chips which are confined in a billet chamber. The heat generated by friction and plastic deformation results in softening of the material; the interparticle gaps are diminished and then the particles are welded together and consolidated.

FSC approach could be compared to sintering based one as they are both based on unidirectional heat flow and mechanical load. But during hot-pressing process, strain and strain rate are very limited comparing to FSC process. Further, FSC provides a better oxide breaking and a better consolidation, at least for given billet heights due to its process mechanics. Besides, the hot-pressing processes have a higher processing time than FSC that could, therefore, represent a more energy efficient recycling route.

However, although fully consolidated billets can be obtained by FSC, these are characterized by non-homogenous mechanical properties and microstructure (Latif et al., 2022). FSC has been also applied for combining different material either to produce Functional Graded Materials (Latif et al. 2022) or to get a new materials with homogeneous and advanced properties (Overman et al., 2021).

The Solid bonding occurrence can be modelled and predicted by implementing solid bonding criteria, these criteria if implemented in numerical codes allows both a process mechanics understanding as well as better process engineering. Basically two different approaches exist for analytically modeling the solid bonding occurrence: the ones based on the energy barrier theory, sometimes referred to as weld criteria, and those that are physically motivated (based on the film theory) (Kolpak et al., 2019).

Concerning the energy barriers models, the first model was developed by Akeret (1992). He assumed that ratio between the contact pressure and the local flow stress must be greater than a critical value

for two metals to be bonded. He applied this criterion to model the bonding of a porthole die extrusion process. The first development of the Akeret model was proposed by Plata and Piwnik (2000), they changed the local and single scalar score into a time dependent formulaton, to be more specific the Plata and Piwnik criterion proposed to integrate over time the Akeret model. The original Plata and Piwnik model has been tested and adapted in different processes. Donati and Tomesani (2004) improved the bonding prediction in the dead zones of an extrusion process by including the local velocity. In fact, the original criterion implementation leads to an overestimation of the weld quality in this areas. The effectiveness of Plata and Piwnik and the Donati and Tomesani criteria were tested also on friction stir welding of aluminum alloys (Buffa et al., 2014) and on Friction Stir Ectrusion processes (Baffari et al., 2017). Ceretti et al. (2009) proved that the threshold value of the Plata and Piwnik criterion depends on the processing temperature, actually they found that this values decrases with increasing temperature. They observed this phenomenon by developing hot flat rolling processes with different temperatures. You et al. (2016) proposed a new formulation including the absolute local temperature, the universal gas constant and the diffusion activation energy. In this criterion, the local strain is taken into account for the first time.
As far as the film theory based bonding criteria models are regarded, the first criterion developed was created by Bay (1979). In his model, the solid bonding occurrence was related to two factors: the expansion of the contact surfaces and the normal contact pressure. For given conditions, local oxide layers breakage occurs leading to a metal micro extrusion that enables material solid bonding. A variation of this model was carried out by Cooper and Allwood (2014); they took into account the shear stress at the interface and the effect of the oxygen captured in the cavities of the material. Concerning the solid bonding criteria specifically developed for chips recycling processes, only two papers have been published so far. The first was proposed by Guley et al. (2013), they modified the Donati and Tomesani criterion by including a shear stress threshold, in fact they assumed that that the solid bonding phenomenon is activated only when a certain critical shear stress value is reached. This threshold ensures the oxide layers between chips to be broken. The authors implemented this new criterion for modelling the chips recycling through porthole die extrusion processes. Recently, Kolpak et al. (2019) adapted the Cooper and Allwood theory to the case of aluminum alloys chips recycling through porthole extrusion. The weld model they proposed allowed to evaluate the quality of the chips bonding with varying die type and hot extrusion parameters.

Overall, the above reported literature review revealed some knowledge gaps:

1/ Although solid bonding criteria have been successfully applied to model the bonding occurrence in solid bonding based processes, they have to be always adapted to the analyzed process. In other words, it does not exist an unique criterion suitable for all the solid bonding mechanics; this means that the analytical formulation and the related tuning of the solid bonding criteria depend on the analyzed process/case study.

2/ In literature, a limited number of papers were published dealing with the solid bonding modelling of chips recycling. One paper dealt with Friction stir Extrusion and two concern the recycling of aluminum alloys chips through porthole die extrusion.

Considering the pressing need of enhancing the knowledge of recycling processes to increase the Technology Readiness Level (TRL) of these kind of manufacturing approaches, in the present paper the solid bonding mechanics of chips recycling through Friction Stir Consolidation is analyzed. To be more specific, the performance of the already available criteria have been analyzed in the case of AA7075 chips recycling. Also, a new and more effective criterion is presented, specifically designed for FSC process. The criteria were tested by implementing a procedure based on experimental data collection, numerical simulations and an optimization procedure implemented in MATLAB environment. The experimental hardness and grain size measurements have been used to analyze the bonding occurrence; the experimental results have been used as refence for testing the different solid bonding criteria.

The structure of the paper consist of four main sections: in section 2 the developed experimental campaign as well as the developed numerical model description are reported, in section 3 the experimental bonding crtierion definition as well as the analysed bonding crieria and the implemented procedure to calculate the threshold values are reported. The results and the validation of the here proposed new bonding criterion for FSC processes are reported in section 4. The main findings are elaborated and summarized in the conclusion section.

2. Materials and methods

2.1 Experimental campaign

During the FSC process, a rotating tool with a proper vertical load is applied to chips batch confined inside a die chamber. The heat is generated by the friction occurring between the rotating tool (see Fig. 1) and the first layer of the chips batch. High temperature, together with plastic deformation due to undergoing rotation and compression, lead to softening of chips, reduction of interparticle gaps enabling solid bonding condition to be achieved.
The starting material was an aluminum alloy AA7075 sheet with a thickness of 3 mm, and chemical composition by mass percentage was 88.07Al-5.07Zn-2.6O-2.25Mg-1.76Cu-0.2Cr-0.03Fe-0.02Mn. The yield strength and tensile strength were 450 MPa and 530 MPa respectively with 12% elongation at break.
The considered alloy was selected due to its popularity in aerospace manufacturing industries, where 90% of the input material turns into machining chips (Allwood et al., 2012) and therefore it is extremely important to recycle them for an efficient use of the resources. In addition, AA7075 represents a class of wrought aluminum alloys with higher hardness value and relatively lower ductility. Thus, analyzing the bonding quality of AA7075 recycled billet can provide a better understanding to forecast the quality of chip welding for relatively soft and ductile alloys. The aluminum sheet was reduced into chips through milling operations with details listed in Table 1.

Table 1 Details of milling process for chips preparation.

Process	Tool	Number of teeth	Rotational speed [RPM]	Feed rate [mm/min]	Depth of cut [mm]
Milling	BDMT11T308ER-JT PR1225	3	1250	280	1

For effective cleaning, chips were submerged for 30 minutes in acetone, which is a commonly used washing solvent for cleaning metal scraps and it is equally applicable both at laboratory and industrial scales. First, 15g chips were loaded in a cylindrical die with a nominal diameter of 25.4 mm and then compacted at 5 kN force by an H13 cylindrical steel tool with a 25 mm diameter. The die and pressing tool system were integrated in a dedicated friction stir welding machine ESAB-LEGIO (Fig. 1). After the pre-compaction, the tool rotation was activated with vertical load starting from 5kN. The load was gradually increased from 5kN to 20 kN with step increment of 0.5 kN/s in 30 seconds. This step was referred to as transition phase. Due to machine limitations, an instant load increment from 5 kN to 20 kN was not possible. In this way, a transition period of 30 seconds was a prerequisite before consolidation step. The productive time was measured once the force reached 20 kN; the time period after 20 kN achievement was referred to as consolidation time. Overall, chips welding was performed at different tool rotational speeds and various lapses of consolidation time according to the experimental plan shown in Table 2. The process parameters were selected based on previous studies (Latif et.al 2022) in accordance with machine load capacity and billet quality. Specifically, the process parameters settings were identified in order to have different levels of unconsolidated areas

in the recycled samples. This choice was driven by the will to test different solid bong criteria on different bonding conditions. Each experiment was repeated three times.

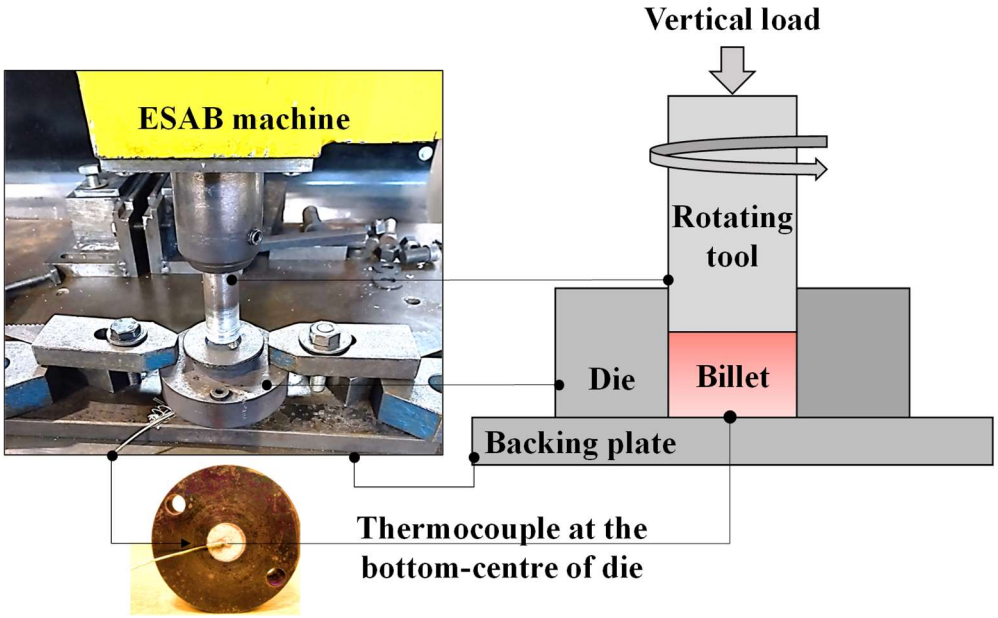

Fig. 1. Friction stir consolidation experimental setup and process sketch.

Table 2 The developed experimental campaign.

Exp ID	Rotational speed [RPM]	Mass [g]	Transition period [s]	Consolidation time [s]
Exp 1	1500	15	30	0
Exp 2	1500	15	30	10
Exp 3	1500	15	30	20
Exp 4	1500	15	30	30
Exp 5	1000	15	30	20
Exp 6	1000	15	30	30

2.2 Measured outputs

For the microstructural analysis and hardness measurement, the samples were first sectioned by using a grinding wheel with low cutting speed. Then the cut samples were mounted by using the compression mounting method. After that, the sectional surface was polished with a series of abrasive papers with grit numbers: P80, P180, P320, P600, P1000, and P12000 by using water to obtain a smooth surface with uniform surface roughness. In the final stage, a polishing cloth of Reflex PAD-MAG, ⌀ 300 mm, NT was applied assisted by silicon carbide as a lubricant. Then, the samples were etched using Keller's reagent (0.5 ml HF, 1.5 ml HCl, 2.5 ml HNO3, and 95.5 ml H2O). GX51 Olympus optical microscope was utilized to analyze the microstructure by using 5x and 50x lenses. The grain size was measured throughout the billet section at 119 observation loci equally spaced at a distance of 1.5mm (Fig. 2). The method of intercept in accordance with the ASTM E112-96 standard test was used by utilizing ImageJ software. The same observation loci were also analyzed for the hardness test. The hardness was measured through the Vickers hardness test by applying HV5 load in accordance with ISO 6507 standard. A load of 49 N (5 kg) was applied for 15 seconds.

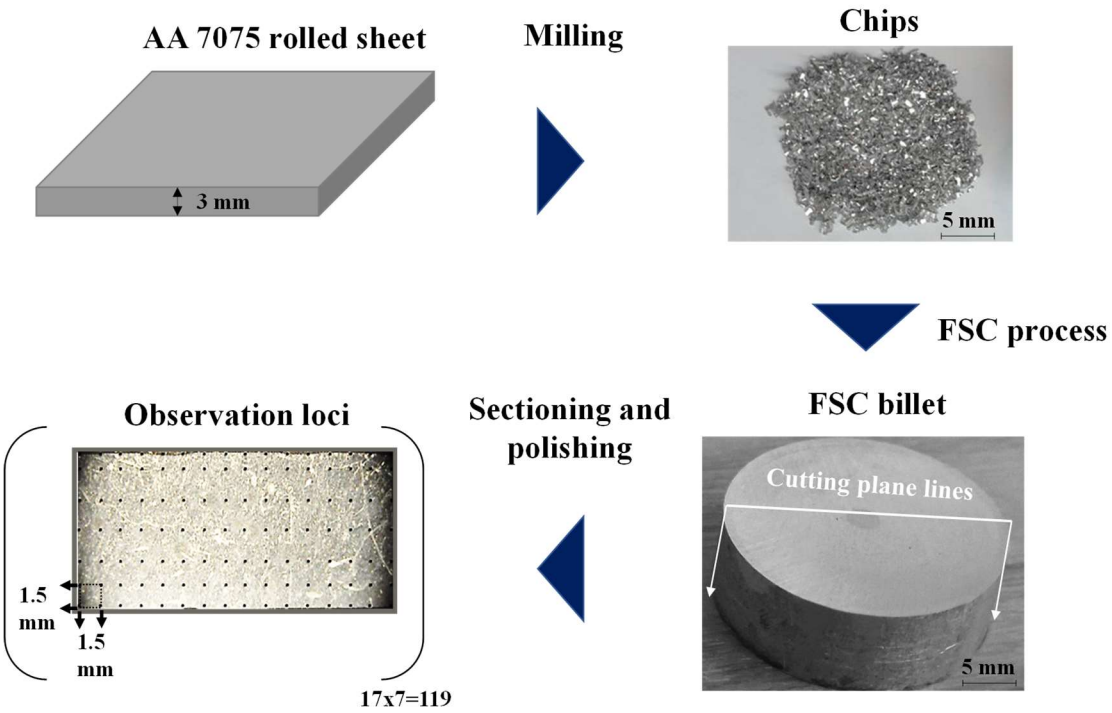

Fig. 2. Different process stages to transform the as-received material AA7075 sheet into FSC solid billet.

2.3 FEM model and validation

The simulation of the FSC process was carried out using the commercial software DEFORM 3D^{TM} , the chips inside the die were considered as a single block chip-based billet and it was modelled as a porous cylinder considering the Shima and Oyane (1976) formulation for porous materials. The porous billet was characterized by a relative density equal to 0.44, the heat transfer coefficient equal to 11 N/sec/mm/C and a mesh of 60000 elements with a refining in the upper surface where the tool contact takes place. The other objects involved in the process were the tool, the die and the backing plate (Fig. 3) that were modelled as rigid parts with a mesh of 15000, 15000 and 35000 elements, respectively. The contacts between the billet and rigid parts were modelled through a friction shear model with a constant shear factor of 0.25. It is worth noting that, although the modeling of the friction conditions can be challenging in friction-based processes, some of the authors of the present paper proved (Buffa et al., 2006) that using a single and constant friction coefficient (shear model) identified by an inverse approach provides reliable results for Friction Stir Welding processes. Therefore, in this research, the friction coefficient was tuned based on the experimental temperature. The selected friction coefficient value was, therefore, identified by an inverse approach, minimizing the error in temperature between experimental and numerical values.

The temperature, strain and strain rate dependent material flow of the considered AA7075 alloy was obtained by both the material database JMatPro (higher temperature stress-strain-strain rate curves) and in house experiments (room temperature stress-strain-strain rate curves). The obtained data have been used to perform a numerical regression and determine the constants shown in the material model (Eq. (1)).

$$\sigma_f = 129 \cdot (\dot{\varepsilon}_0 - \bar{\varepsilon}^{\,0.201}) \cdot \dot{\varepsilon}^{\,0.002} \cdot exp^{441/T} \quad (1)$$

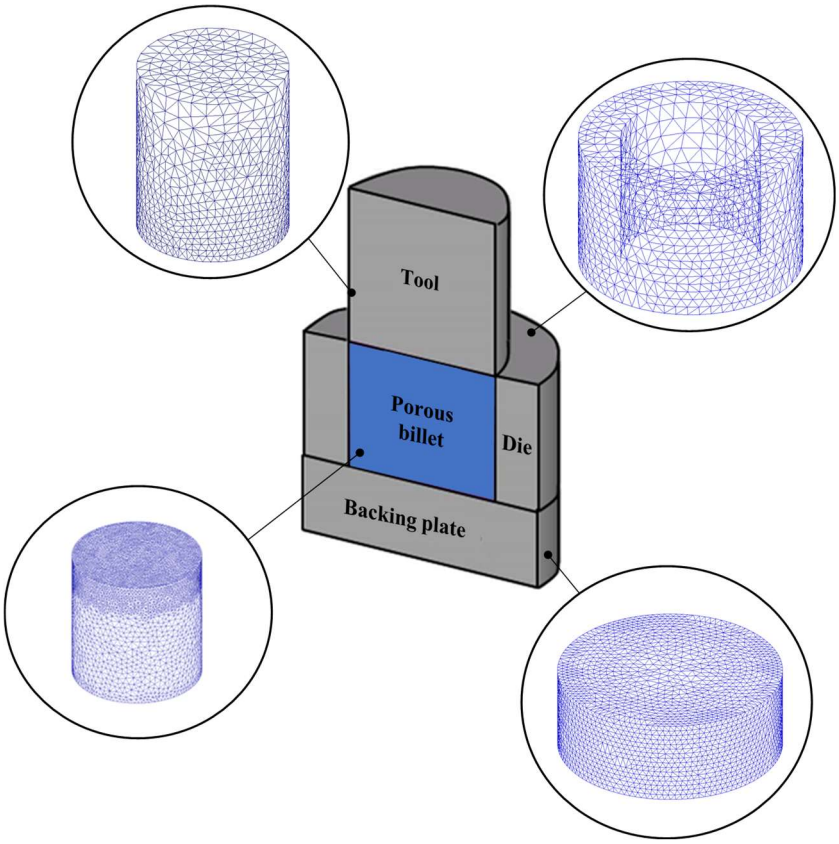

Fig. 3. Numerical model for tool, die, backing plate and porous billet.

The numerical simulation was carried out using a force-controlled tool characterized by a vertical load obtained from the experimental tests and a rotational speed equal to 1500 rpm. The duration of this process was settled to 60s. To ensure the reliability of the numerical results, the experimental velocity and the displacement of the tool were compared to the numerical ones; the results shown in Fig. 4 proves a good matching between the experimental measurement and the numerical prediction. To further test the reliability of the numerical model, a thermocouple was used to record the temperature at the bottom-center of the chips-based billet, also in this case the numerical tool provided a successful prediction (see Fig. 5).

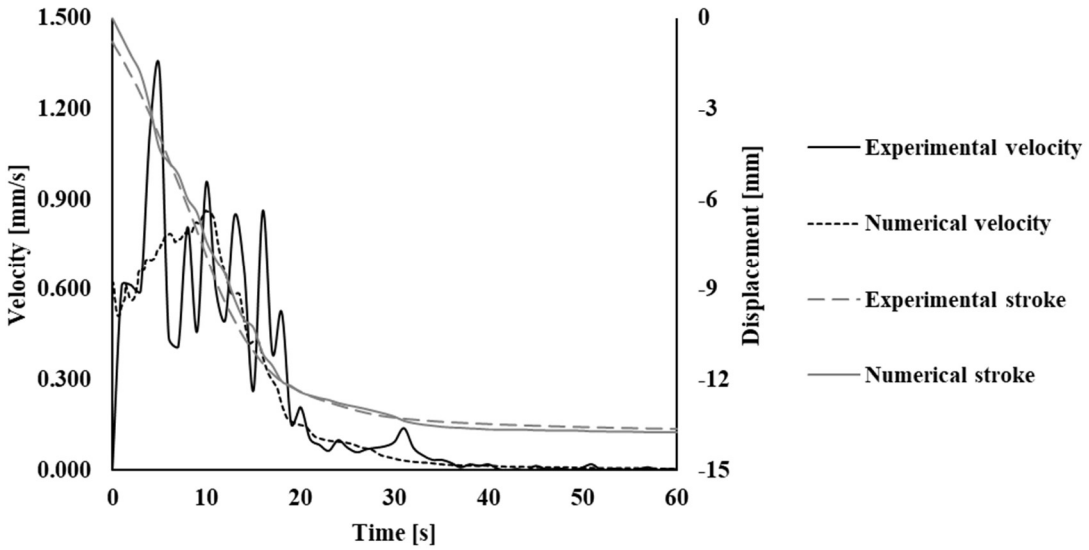

Fig. 4. Experimental and numerical velocity and displacement comparison for numerical-simulation tuning.

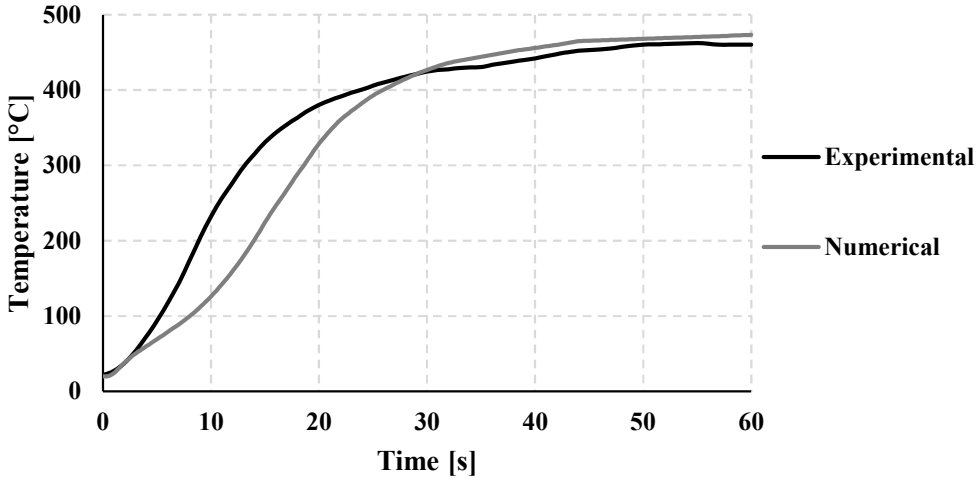

Fig. 5. Comparison between experimental and numerical temperature profile during FSC at bottom-center of the billet.

3. Experimental and numerical bonding criteria definition

In this section the procedures for the experimental bonding criterion definition and the numerical bonding criteria implementation are described. In section 3.1 the experimental approach based on hardness and grain size analyses, for the experimental campaign described in Table 2, is reported. The output of the experimental campaign allowed the definition of an experimental bonding criteria that was used as benchmark for the numerical bonding criteria testing and design. This latter aspect is reported in section 3.2 and 3.3, to be more specific section 3.2 contains the description of all analyzed solid bonding criteria. In section 3.3 the automatic procedure for the threshold limit (W_{Ci}^{lim}) calculation of each analyzed criterion is reported.

3.1 Experimental bonding criterion

In order to test various numerical models predicting the quality of chips welding during FSC, it is important to quantitatively evaluate the bonding prediction performance of each numerical model with a respect an experimental reference. For this reason, a reference experimental benchmark was developed based on two measured outputs: hardness value and average grain size.

The hardness measurement takes into account indirectly several quality indicators such as degree of chips compaction, density, material strength etc. In the similar way, grain size qualitatively depicts the desired amount of heat, temperature and strain rate. The authors have also recently found a good matching between hardness distribution and local compression strength of recycled FSC samples (Latif et al., 2023). Therefore, it is expected that a threshold based on hardness value and grain size can provide a broad understanding about consolidation and can be used for developing the foundation for experimental bonding reference.

From now on the identified reference will be referred to as experimental bonding criterion. This criterion was framed out after a detailed investigation of three different objects: as-received material, compacted chips obtained from milling operation, and manufactured FSCed solid billet.

First, the starting material (as-received material) AA7075 sheet was fully analyzed. Average values of 150 HV and 155 µm were noticed for hardness and grain size, respectively.

In the next step, AA7075 sheet was reduced into chips and the microstructure of chips was investigated in to order to know the changes caused by the milling process. Due to the process mechanics of the milling operation, the average grain size was significantly reduced to a range of 0.5-2 µm. However, the hardness value was not measured because pre-processed compacted chips were in the form of a porous material with a relative density equal to 0.44. However, for each individual

chip, a relatively higher hardness value is expected due to the milling operation as reported by Rofman et al (2019).
Finally, chips were consolidated into a solid cylindrical billet during FSC process. A detailed investigation was performed on 119 different observation loci to analyze the microstructure and hardness distributions obtained after FSC step. Based on the values measured in such loci, hardness values, and grains size distributions were interpolated to obtain the consolidated/non-consolidated areas as reported in (Fig. 6 step 2 and 3).

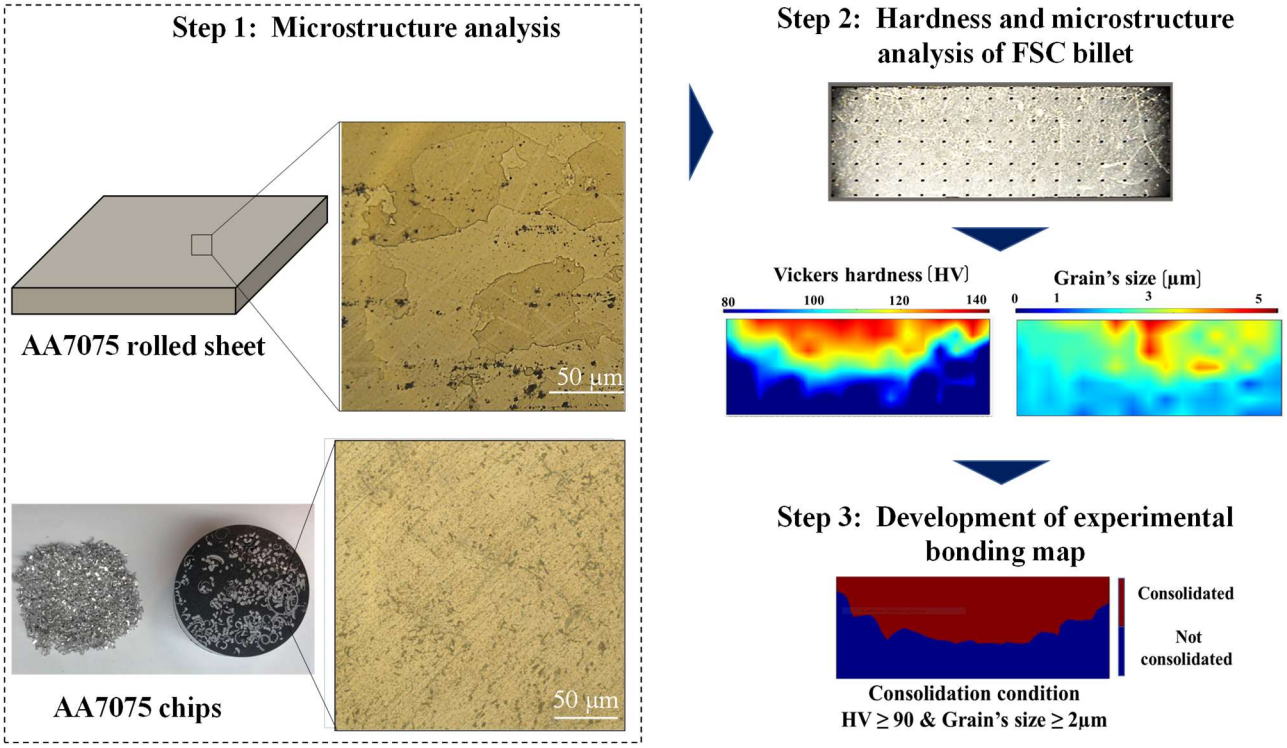

Fig. 6. Steps for experimental bonding criteria definition.

In the bottom section of the billet the microstructure was found similar to the pre-processed chips with several defects such as visible chips boundaries, voids, cavities, cracks, etc. (Fig. 7); the average grains size fell within the range of 0.5-2 µm. This indicates that the microstructure of the bottom part remained unaltered during the FSC process. Moving toward the top part of the billet, changes in microstructure (grain growth) and the improvement in billet quality (disappearance of defects) were noticed. It was quite evident that these changes occurred specifically at grain size exceeding 2 µm. To ensure the achievement of the full consolidation condition, a minimum hardness value of HV 90 (60% of as-received material) was also considered on the bases of experimental evidences. At this hardness value, the billet showed good consolidation without any defects like visible chips boundaries, voids, cavities, cracks, etc. In this way, an idea of experimental bonding condition was evolved by taking into account the combined effect of microstructure and hardness values.

The definition of experimental criteria for the AA7075 alloy is, therefore, formulated as follows:

"Any zone on the FSC billet section that has an average grain size at least equal to the maximum average grain size of the unprocessed chip (2 µm) AND the hardness value of at least 60% of the as-received material hardness (HV 90) is labeled as fully consolidated".

As already stated, the different process parameters settings allowed to achieve different levels of consolidation, actually by increasing the processing time (moving from Exp 1 to Exp 4) the consolidation front moves downwards by expanding the consolidated portion of the billet (Li et al.

2018). This aspect will be clearly visible looking at the hardness and grain sizes maps presented in section 4, nevertheless in Fig. 8 the difference in terms of defect occurrence between Exp 1 and Exp 4 is visible.

In the case of Exp 1, several defects such as cavity and chip boundaries were noticed as shown in Fig. 8a. On the other hand, when the processing time was increased to 60 seconds in Exp 4 (Fig. 8b), the consolidated area started to expand, and the defective zone got diminished.

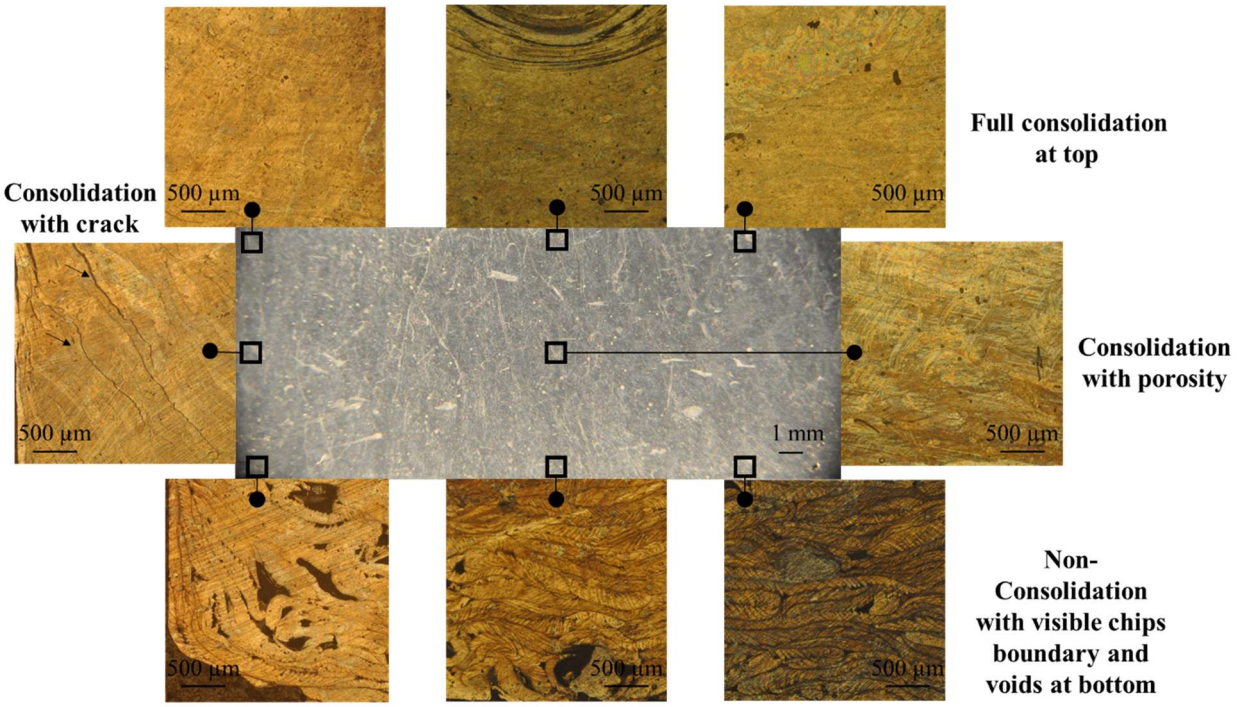

Fig. 7. Detailed microstructure analysis for Exp 1 (5X Lens)

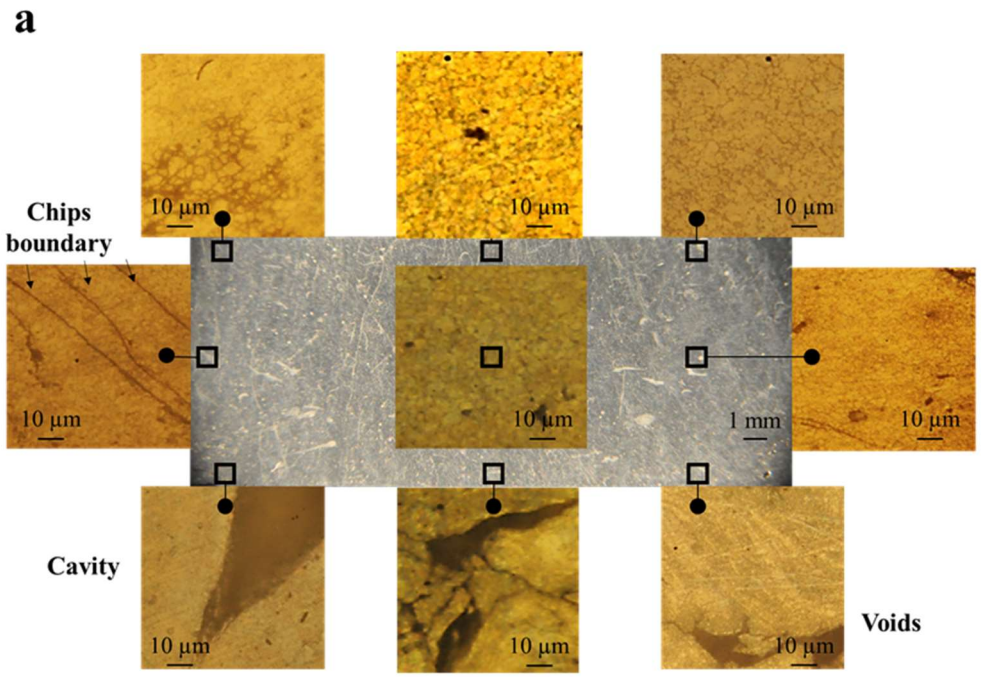

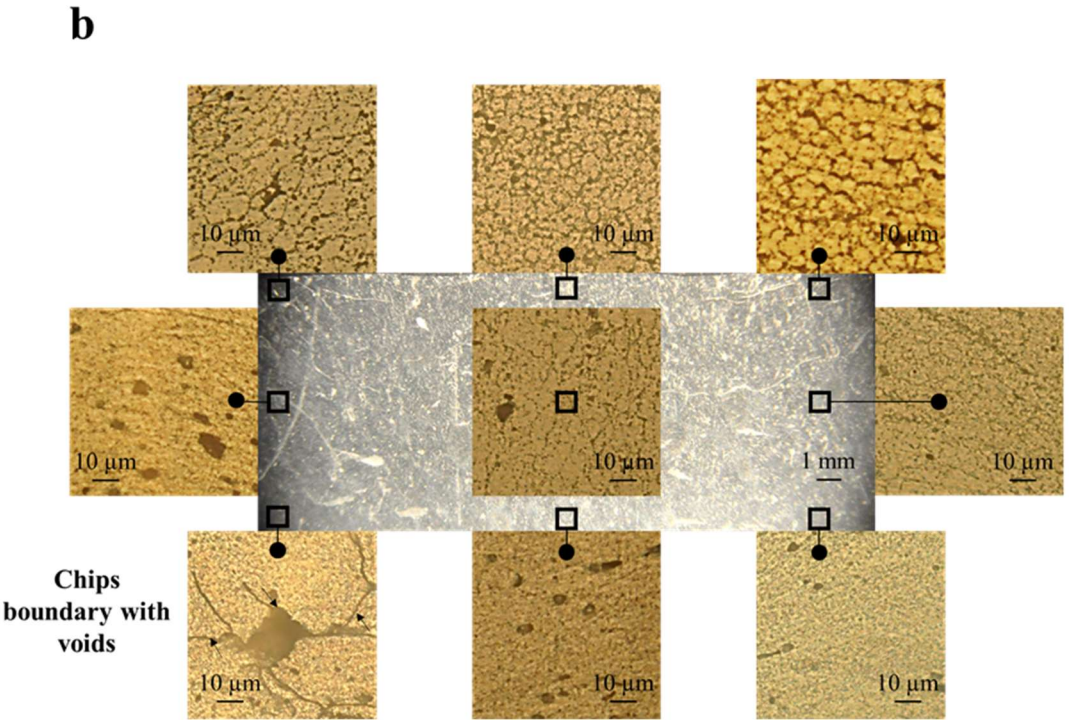

Fig. 8. Microstructure of AA7075 FSC billet section for (a) Exp 1 and (b) Exp 4 (50X Lens)

3.2 Numerical bonding criteria

Together with the bonding criteria already available in literature, two more bonding criteria are here proposed and analyzed. The first new criterion is reported in Eq. (2) where the Zener – Hollomon parameter was included in the Plata – Piwnik criterion. The Zener – Hollomon parameter is related to the recrystallization of the material and it takes into account the effect of the temperature compensated strain rate in the consolidation process. Overall, the aim was to analyze if the inclusion of a factor related to grain size and recrystallization would improve the solid bonding occurrence prediction during FSC.

$$W_{C6} = \int_{t_0}^{t_f} \frac{|\sigma_{mean}|}{\sigma_f} \cdot \frac{1}{Z} dt \tag{2}$$

This criterion was tested considering a temperature activation threshold (480 °C); in other words, as the temperature of the tracked point is below this threshold, the bonding value (W_{C6}) was considered equal to zero (see Eq. (3)). This temperature threshold was identified with an iterative approach in order to optimize the matching between the experimental results and the predicted ones obtained with the adopted solid boning criterion (the procedure was implemented on all the experiments from 1 to 4).
This assumption was defined in order to avoid the excessive growth of the W value because of the "stationarity" of the FSC process as further explained in section 4.

$$\begin{cases} W_{C6} = \int_{t_0}^{t_f} \frac{|\sigma_{mean}|}{\sigma_f} \cdot \frac{1}{Z} dt & T \geq 480\ °C \\ W_{C6} = 0 & T < 480\ °C \end{cases} \tag{3}$$

The used threshold was chosen on the basis of the optimization procedure aimed to maximize the overlapping between the experimental results and the numerical predictions.

The second developed criterion (see Eq. (4)) involves the use of two parameters which can be defined "weights" of the bonding criterion. The main aspect of these parameters is the capability to emphasize the bonding in that material zones where temperature and the strain changes occur synergistically. These parameters are expressed as the ratio between the variation of the variable over a given time span (equal to the simulation time step) and the value of the same variable at simulation step *i*. In this research, the time span was considered equal to 0.05 s.

$$W_{C5} = \int_{t_0}^{t_f} w_s \cdot w_T \cdot \frac{|\sigma_{mean}|}{\sigma_f} dt \tag{4}$$

where w_T and w_s (see Eq. (5)) are the weights of the temperature and of the strain, respectively; *i* is the considered simulation step and σ_f is the material flow stress.

$$w_T = \frac{T_i - T_{i-1}}{T_i} = \frac{\Delta T}{T_i} \qquad w_s = \frac{\varepsilon_i - \varepsilon_{i-1}}{\varepsilon_i} = \frac{\Delta \varepsilon}{\varepsilon_i} \tag{5}$$

All the criteria analyzed in the present paper are listed in Table 3, both the original equations (named in Table 3 Literature equation) and the adopted equations are reported. Specifically, the mean stress absolute value and effective stress were used in place of the contact pressure and the flow stress, respectively. In order to calculate the different criteria in the 119 observation loci of the cross section, the track point procedure was used. This procedure allows to evaluate the evolution of the considered field variables and of the material flow stress for each of the 119 observation loci. The different integrals reported in Table 3 were, therefore, numerically calculated using the trapezoidal rule (Donati and Tomesani, 2004).

Table 3 Bonding criteria equations.

ID	Criterion	Literature equation	Adopted equation
C1	*Akeret (1992)*	$W_{C1} = \frac{p}{\sigma_f}$	$\frac{\lvert\sigma_{mean}\rvert}{\sigma_f}$
C2	*Plata and Piwnik (2000)*	$W_{C2} = \int \frac{p}{\sigma_f} dt$	$W_{C2} = \int \frac{\lvert\sigma_{mean}\rvert}{\sigma_f} dt$
C3	*Donati and Tomesani (2004)*	$W_{C3} = \int \frac{p}{\sigma_f} dt \cdot v$	$W_{C3} = \int \frac{\lvert\sigma_{mean}\rvert}{\sigma_f} dt \cdot v$
C4	*Kolpak et al. (2019)*	$W_{C5} = \frac{\sigma_{b.n}}{\sigma_f, n} = max\left(\frac{\sigma_{b,i}}{f, i}\right)$	$W_{C4} = \frac{\lvert\sigma_{mean.n}\rvert}{\sigma_f, n} = max\left(\frac{\lvert\sigma_{mean,i}\rvert}{\sigma_{f,i}}\right)$
C5	*Plata - Piwnik – Weighted*	New formulation	$W_{C5} = \int w_t \cdot w_s \cdot \frac{\lvert\sigma_{mean}\rvert}{\sigma_f} dt$
C6	*Plata - Piwnik – Zener*	New formulation	$W_{C6} = \begin{cases} 0, & T < 480 \\ \int \frac{\lvert\sigma_{mean}\rvert}{\sigma_f} \cdot \frac{1}{z} dt, & T \geq 480 \end{cases}$

3.3 Numerical bonding threshold values calculation procedure

For each criterion a threshold value (W_{Ci}^{lim}, where i = 1, 2, … , 6) for predicting the bonding condition occurrence was calculated. The W_{Ci}^{lim} was calculated with the iterative model depicted in Fig. 9. For each criterion and for each analyzed consolidation time (Exp 1 to 4 of Table 1), the W_{Ci}^{lim} identifying the fully consolidated area needs to be calculated. In this respect, an automatic procedure able to calculate the W_{Ci}^{lim} providing the best fitting with experimental results was designed and implemented. This procedure integrates experimental data with numerical results through a minimization algorithm implemented in MATLAB environment. The purpose of this model is to

create an automatic and more accurate calculation process for the identification of the bonding criterion threshold (W_{Ci}^{lim}).

The steps of the developed procedure are reported in the flow chart depicted in Fig. 9.

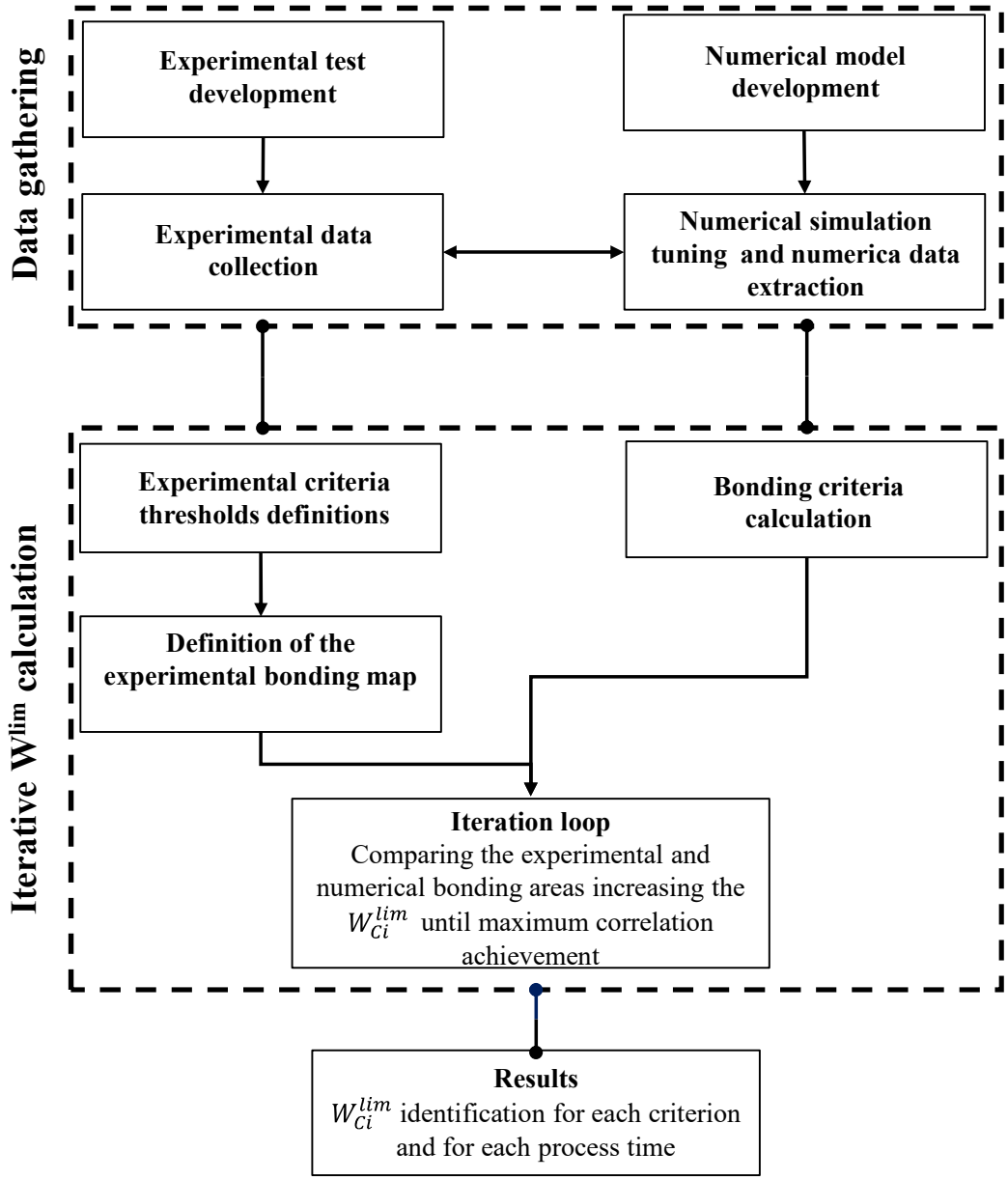

Fig. 9. Implemented workflow for automatic W_{Ci}^{lim} calculation.

The iteration cycle starts with the data gathering phase. In this step hardness and grain size of the four samples (see Table 2, Exp 1 to 4), as described in section 3.1, were collected. In the meantime, the values of the main variables related to bonding occurrence were extracted from the numerical results. Specifically, the variables were extracted for the 119 loci (see Fig. 2) in order to have an effective matching between experimental and numerical observations. In this respect, the matrix of numerical points (observation loci), used for developing the points tracking and following the evolution of the field variables, was the same for both experimental and numerical cross sections.

Once the experimental data were acquired two different matrixes containing the hardness and the grain size values for the 119 analyzed observation loci have been created for the Exp 1 to 4. These matrixes allow maps of hardness (Fig. 10a) and grains size (Fig. 10b) of the cross sections of the analyzed samples to be obtained.

As explained in section 3.1, for the analyzed aluminum alloy specific hardness and grain size thresholds were identified, according to this criterion two specific regions can be identified in the sample's cross sections:

- Consolidated area: the area where the value of both hardness and grain size exceeds the hardness and the grain size thresholds previously identified (see definition of experimental criteria in section 3.1).
- Not consolidated area: the area where neither the hardness nor grain size values reach the value of the thresholds previously identified.

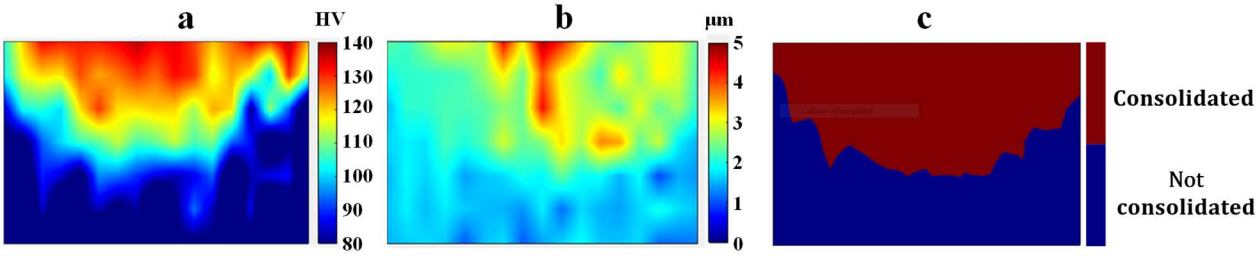

Fig. 10. Example of colored map for (a) hardness, (b) grain size and (c) derived experimental bonding map for Exp 1.

The next step concerns the bonding criteria calculation; using all the field variables extracted from the simulation the bonding criterion value has been calculated for each of 119 loci, for each Exp 1 to 4. Once the values of the numerical criteria are available, the iteration procedure can be initialized according to the following steps.

1. Setting the scale limit of the numerical bonding map equal to a bonding limit value (W_{Ci}^{lim}). For the first step of the iteration the W_{Ci}^{lim} value was set equal to zero.
2. Incrementally increasing of the W_{Ci}^{lim} value and check the area similarity between the experimental bonding map and the numerical bonding map using an image comparison approach available on MATLAB. The similarity has the meaning of correlation coefficient (r) calculated in the following way (Eq. (6)):

$$r = \frac{\sum_m \sum_n (A_{mn} - \bar{A})\,(B_{mn} - \bar{B})}{\sqrt{(\sum_m \sum_n (A_{mn} - \bar{A})^2)(\sum_m \sum_n (B_{mn} - \bar{B})^2)}} \quad (6)$$

   Where A and B are the logical array representative the two maps, m and n are the elements of the array, $\bar{A}$ and $\bar{B}$ are respectively the mean value of A and B.

   The procedure is stopped when the maximum correlation, i.e., when the best overlapping between experimental and numerical bonding area, are reached.

3. Obtainment of the optimal W_{Ci}^{lim} values and of the corresponding correlation coefficients.

The procedure was implemented for the six criteria reported in Table 3 and for all the case studies reported in Table 2.

4. Discussion of the results

In this section, the obtained results of both the experimental procedure and the numerical bonding criteria calculation are discussed for the process conditions Exp 1, Exp 2, Exp 3 and Exp 4 of Table

2. In Fig. 11, the observed hardness and grain size distributions along with the derived experimental bonding maps are reported.

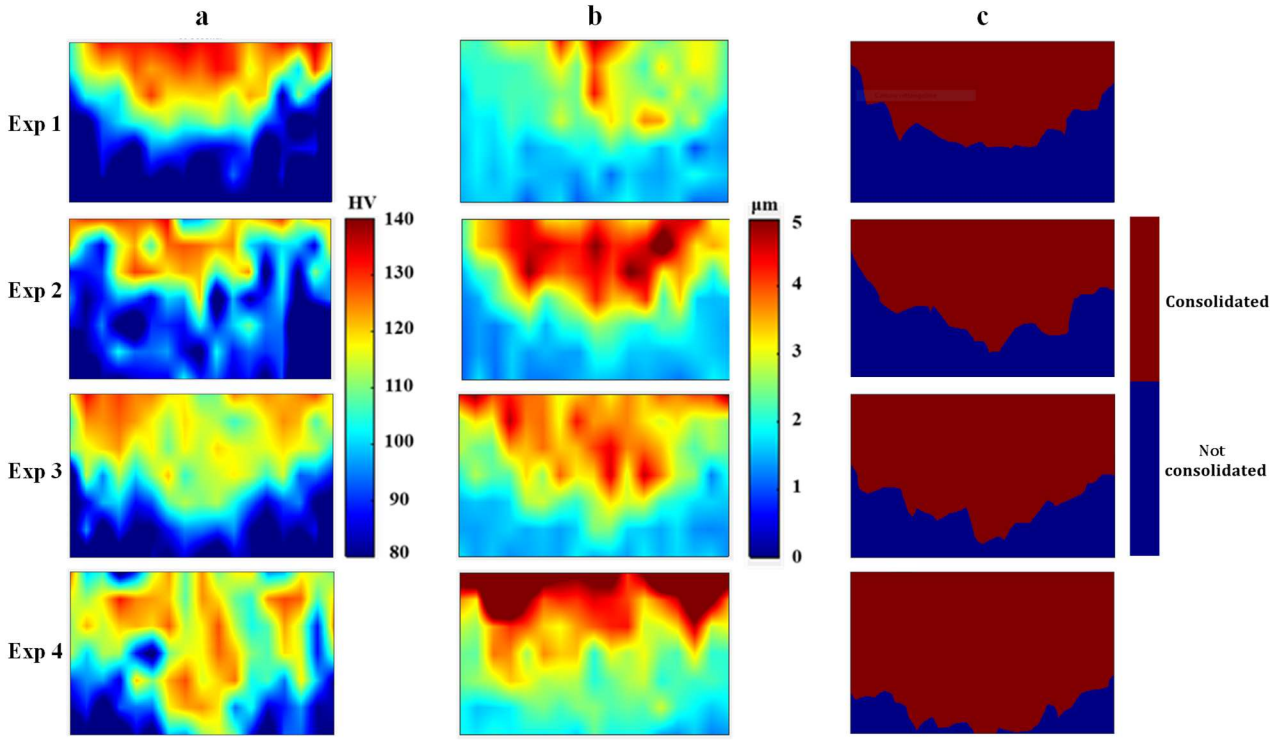

Fig. 11. (a) Hardness, (b) grain size distributions and (c) experimental bonding maps for Exp 1, Exp 2, Exp 3 and Exp 4.

Since moving from Exp 1 to 4 the consolidation time increases from 0s to 30s, it is possible to notice that increasing the processing time the bonding area significantly increases. Specifically, the consolidation front moves downwards according to the heat and strain evolution over time (Li et al., 2018). In fact, an axisymmetric heat flow moving from the top toward the bottom occurs, moreover the die and the backing plate serve as a heat sink, reducing the temperature and constraining the deformation of nearby aluminum alloy chips (Tang and Reynolds, 2011). In conclusion, the farther the chips are from the top (rotating tool) the more difficult are the solid bonding conditions to be achieved.

In the analyzed case studies, it is possible to notice, that even with the maximum consolidation time, a fully consolidated billet was not obtained. Actually, a non-consolidated region is still visible at the bottom of the Exp 4 experimental bonding map of Fig. 11.

The numerical bonding map obtained by means of the optimization procedure described in section 3.3 are shown in Fig. 12 and Fig. 13. The different maps represent the material bonding criteria distribution for different consolidation time 0, 10, 20 and 30 seconds. To better highlight the bonding zone and to provide a better comparison between the numerical and the experimental bonding maps, the maximum value of the numerical bonding maps scale was set equal to the W_{Ci}^{lim} found. This particular setting allows to create a dark red zone characterized by values that are greater or equal to the W_{Ci}^{lim}, thus representing a fully consolidated region. The different calculated W_{Ci}^{lim} for each criterion and for each consolidation time are reported in Table 4. In this table the correlation coefficient values as described in section 3 are also listed. It is possible to notice that C1, C2 and C4 are characterized by poor values of the correlation coefficient, and this results in a not reliable bonding map evolution as visible in Fig. 12 and Fig. 13. On the other hand, C3, C5 and C6 maps, although characterized by different bonding region shapes, provide a good matching between the experimental

bonding criterion and the numerical predicted one. Nevertheless, as it is possible to notice from Fig. 12 and Fig. 13, the W_{Ci}^{lim} is not a constant value but varies with varying the considered consolidation time and this happens for each analyzed criterion. In other words, it is not possible to find a unique W_{Ci}^{lim} value with varying processes conditions (temperature, strains, stress status, etc.). To further highlight such assumption the test provided in Fig. 14 was developed. Specifically, in Fig. 14a the bonding map (for the Plata – Piwnik – Zener criterion) is reported for the 0 second consolidation time (Exp 1) using the calculated 30 seconds consolidation time (Exp 4) W_{C6}^{lim}. It is possible to notice that the obtained map does not predict at all the bonding occurrence; in fact, the identified W_{C6}^{lim} underestimates the bonding occurrence significantly. On the other hand, in Fig. 14b the bonding map for the Exp 4 using the calculated Exp 1 W_{C6}^{lim} is reported, also in this case the prediction is not reliable as the W_{C6}^{lim} overestimates the bonding occurrence. This misleading result was observed for all of the analyzed criteria.

In conclusion, the use of a single value for different process times does not provide a reliable bonding occurrence prediction, as a matter of fact either over-estimation or under-estimation of the bonding occurrence was observed. What described for the Plata – Piwnik – Zener was observed all the same for the six criteria here analyzed. This result was somehow expected, actually in literature has been already proved the dependence of the W_{Ci}^{lim} on the temperature, to be more specific Ceretti et al. (2009) proved for instance that W_{C2}^{lim} decreases with increasing the processing temperature in a port hole extrusion process. This result can be easily explained as with increasing temperature the required activation energy for bonding decreases and, thus, the value W_{C2}^{lim} decreases as well.

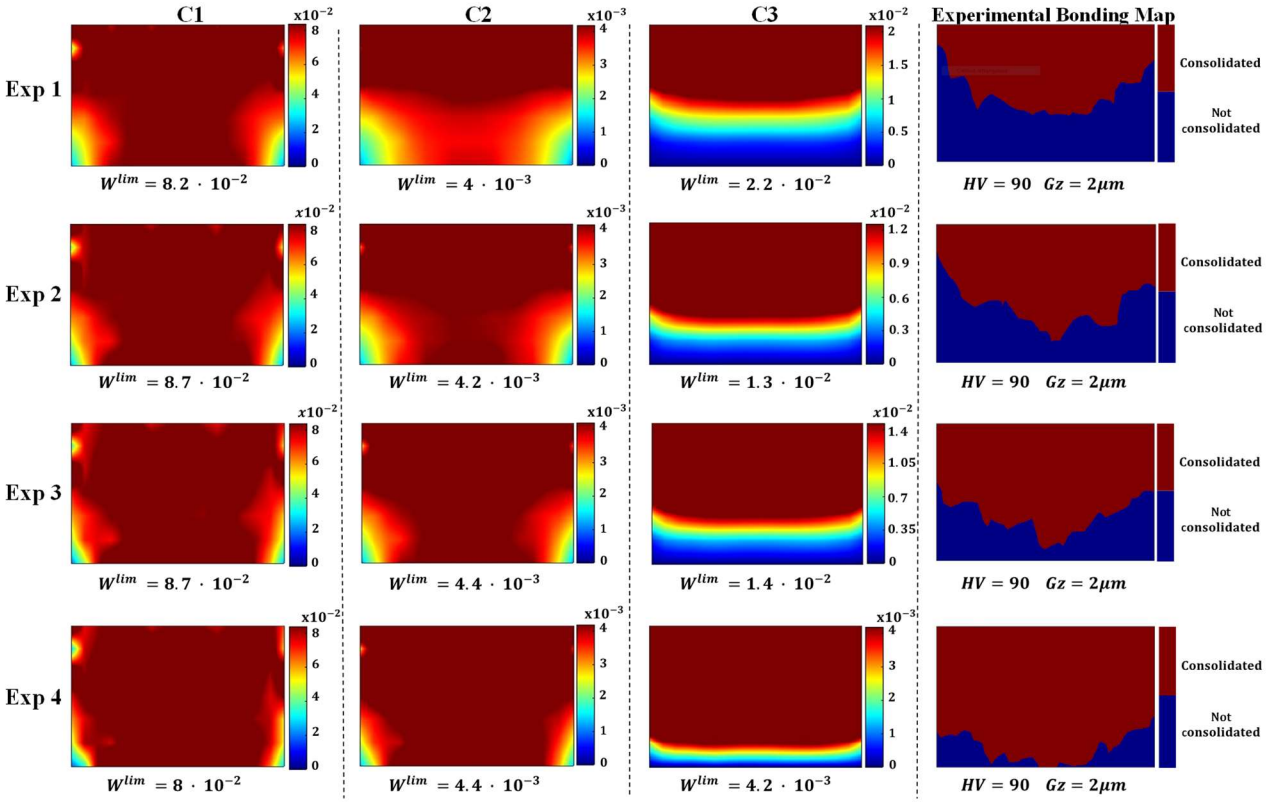

Fig. 12. Numerical bonding maps for Akeret (C1), Plata – Piwnik (C2), Donati and Tomesani (C4) criteria and experimental bonding maps.

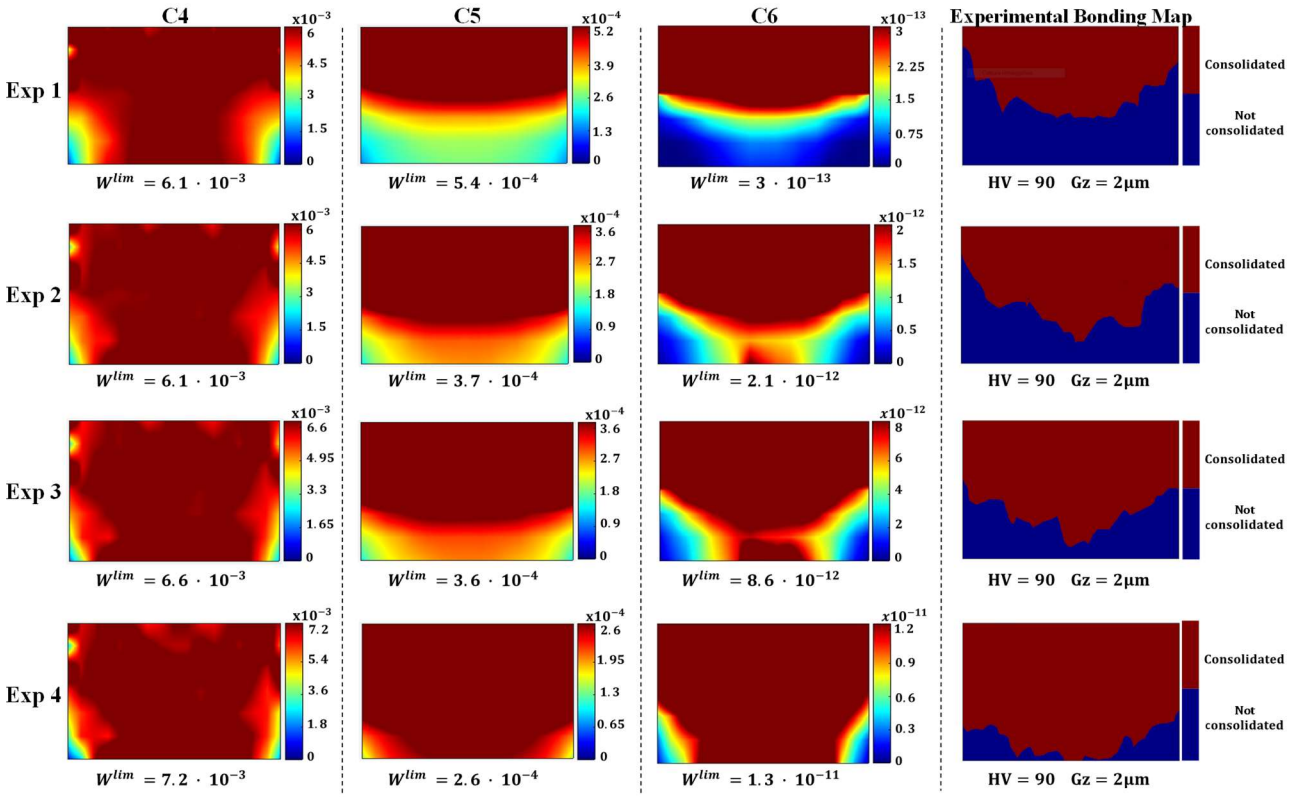

Fig. 13. Numerical bonding map for Kolpak et al. (C4), Plata – Piwnik weighted (C5) Plata – Piwnik - Zener (C6) criteria and the experimental bonding maps.

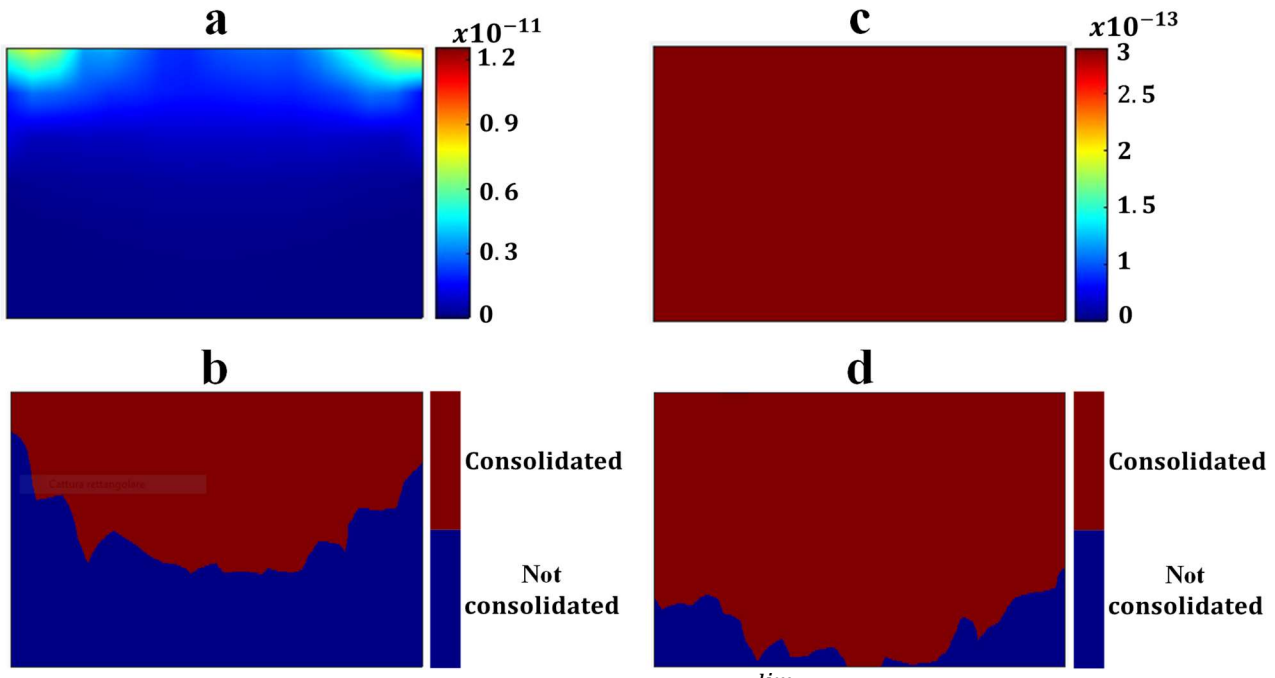

Fig. 14. (a) Exp1 numerical bonding map based on W_{C6}^{lim} calculated for Exp 4, (b) Exp1 experimental bonding map, (c) Exp 4 numerical bonding map based on W_{C6}^{lim} calculated for Exp 1 and (d) Exp 4 experimental bonding map.

A better overview of these trends is provided with the graphs reported Fig. 15. In these graphs the value of the bonding limit W_{Ci}^{lim} versus the mean temperature values of the bonding line are reported. It is possible to notice that the bonding limit value W_{Ci}^{lim} for most of the criteria increases with increasing temperature, this trend is quite unrealistic considering the solid bonding physics,

questioning the effectiveness of some of the tested criteria. Looking at the results of Fig. 15, the only criteria characterized by a decreasing trend with increasing temperature are C3 and C5. These criteria, in fact, can better take into account the peculiar solid bonding mechanics of FSC.

Table 4 Values of maximum correlation coefficients and the corresponding W_{Ci}^{lim} for Exp 1, Exp 2, Exp 3 and Exp 4.

Criterion	Exp ID	Correlation coefficient [%]	W_{Ci}^{lim}
Akeret (C1)	Exp 1	51	$8.2 \cdot 10^{-2}$
	Exp 2	64	$8.7 \cdot 10^{-2}$
	Exp 3	51	$8.7 \cdot 10^{-2}$
	Exp 4	40	$8.0 \cdot 10^{-2}$
Plata – Piwnik (C2)	Exp 1	49	$4.0 \cdot 10^{-3}$
	Exp 2	58	$4.2 \cdot 10^{-3}$
	Exp 3	51	$4.4 \cdot 10^{-3}$
	Exp 4	39	$4.4 \cdot 10^{-3}$
Donati – Tomesani (C3)	Exp 1	95	$2.2 \cdot 10^{-2}$
	Exp 2	77	$1.3 \cdot 10^{-2}$
	Exp 3	89	$1.4 \cdot 10^{-2}$
	Exp 4	87	$4.2 \cdot 10^{-3}$
Kolpak et al. (C4)	Exp 1	57	$6.1 \cdot 10^{-3}$
	Exp 2	65	$6.1 \cdot 10^{-3}$
	Exp 3	60	$6.6 \cdot 10^{-3}$
	Exp 4	48	$7.2 \cdot 10^{-3}$
Plata – Piwnik – Weighted (C5)	Exp 1	96	$5.4 \cdot 10^{-4}$
	Exp 2	82	$3.7 \cdot 10^{-4}$
	Exp 3	88	$3.6 \cdot 10^{-4}$
	Exp 4	98	$2.6 \cdot 10^{-4}$
Plata - Piwnik – Zener (C6)	Exp 1	94	$3.0 \cdot 10^{-13}$
	Exp 2	84	$2.1 \cdot 10^{-12}$
	Exp 3	87	$8.6 \cdot 10^{-12}$
	Exp 4	84	$1.3 \cdot 10^{-11}$

Note: Akeret W_{C1}^{lim} [Mpa/MPa], Plata - Piwnik W_{C2}^{lim} [s], Donati - Tomesani W_{C3}^{lim} [mm], Kolpak et al. W_{C4}^{lim} [Mpa/MPa], Plata – Piwnik – Weighted W_{C5}^{lim} [s], Plata - Piwnik – Zener W_{C6}^{lim} [s^2].

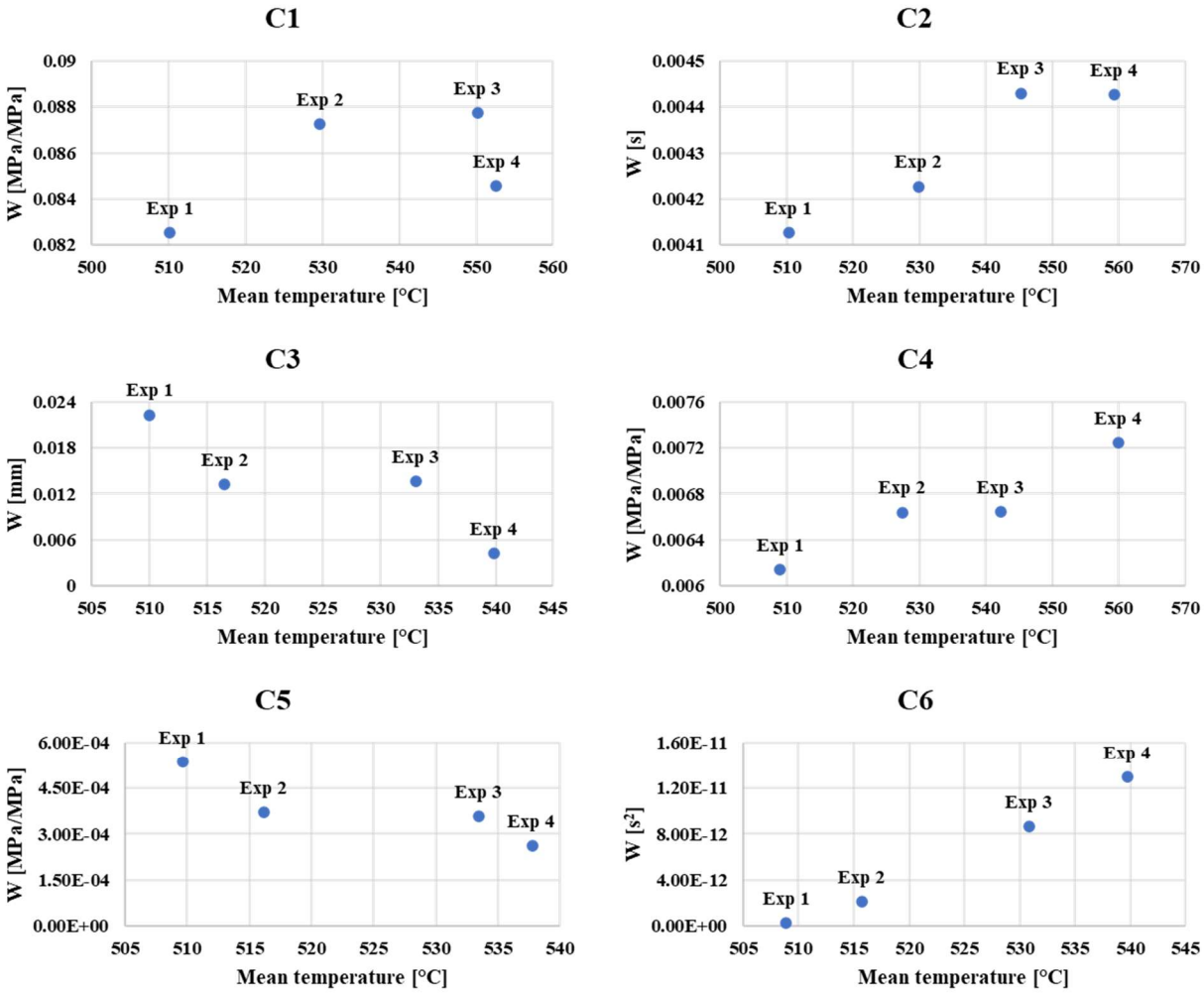

Fig. 15. Calculated W_{Ci}^{lim} values versus temperature trends for each analysed criterion.

As a matter of fact, the chips-based billet remains inside the die for the entire process duration, consequently the value of a given bonding criterion (W) steadily increases throughout the FSC process. This causes the W_{Ci}^{lim} threshold to be reached also for regions of the billet that could never reach actual solid bonding conditions. This phenomenon is similar to what analyzed in the dead material zone by Donati and Tomesani (2004), for the case of port hole die extrusion. Moreover, from the results of the numerical simulation it is possible to notice that the effective strain and nodal velocity values are characterized by limited values and variation especially during the consolidation phase (from 30 to 60 seconds processing time) (Fig. 16). It is worth remarking that in Fig. 16 the nodal local velocity is reported, and a clear decreasing trend is visible (the maximum values of the colored scale was changed accordingly). These results support the assumption that the FSC process somehow resembles the dead zone analyzed by Donati and Tomesani (2004), hence changes in the classical bonding criteria are needed. To be more specific, the criteria that provide the best performance (C3 and C5) have been thought with the idea to limit the constant summation of the solid bonding criterion where temperature, strain and strain rate gradient values are low. This is obtained by the introduction of factors v, w_s and w_t for the C3 and the C5 criterion, respectively.

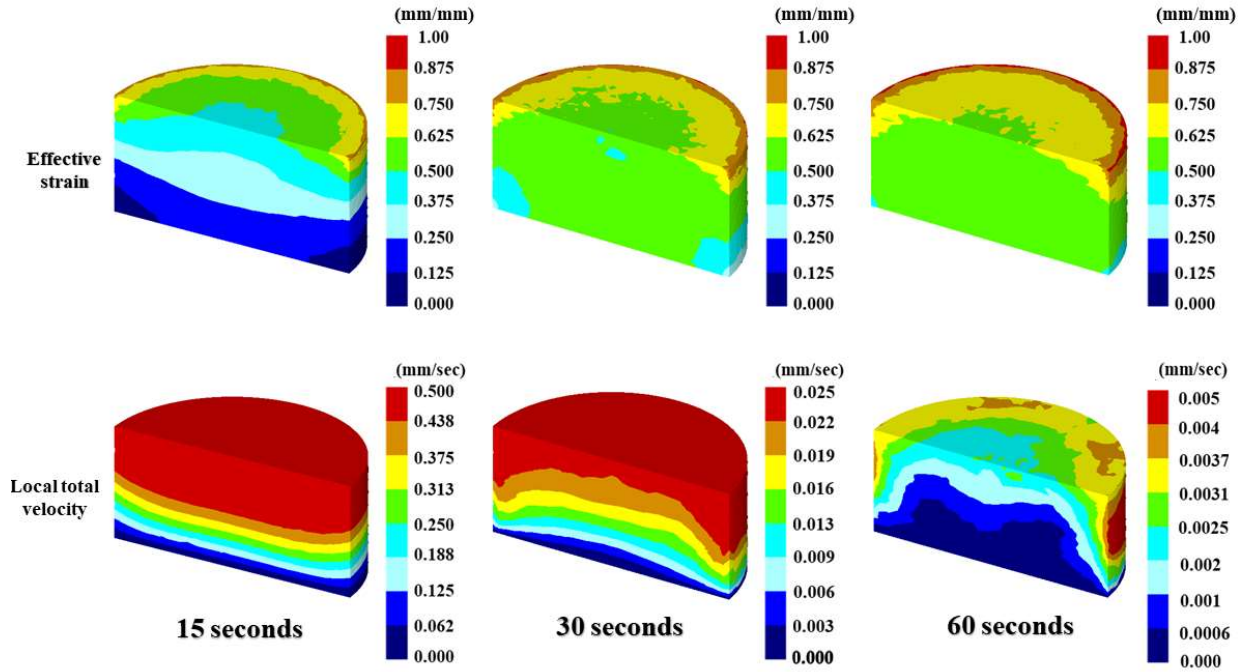

Fig. 16. Effective strain and local velocity for 15, 30 and 60 seconds processing time (transition time and consolidation time).

4.1 Validation of the new solid bonding model for the FSC

In order to evaluate the prediction performance of the analyzed solid bonding criteria for FSC, two additional experiments were performed by using 1000 rpm, 20 kN, with total processing time of 50 and 60 seconds (Exp 5 and 6, see again Table 2).With these process parameters setting, the heat generated by friction is slightly reduced leading to a reduction in maximum temperature achievement. Therefore, a smaller consolidation area is obtained for a given consolidation time compared to the experiments developed with 1500 rpm. This choice was driven by the will to test the model on different conditions with respect to the ones the model was built on. The difference of the experimental bonding criterion of the 50 seconds processing time obtained with different RPM (Exp 3 and 5) is reported in Fig. 17; also, the difference in temperature distribution is reported in the numerical temperature map of Fig. 18.

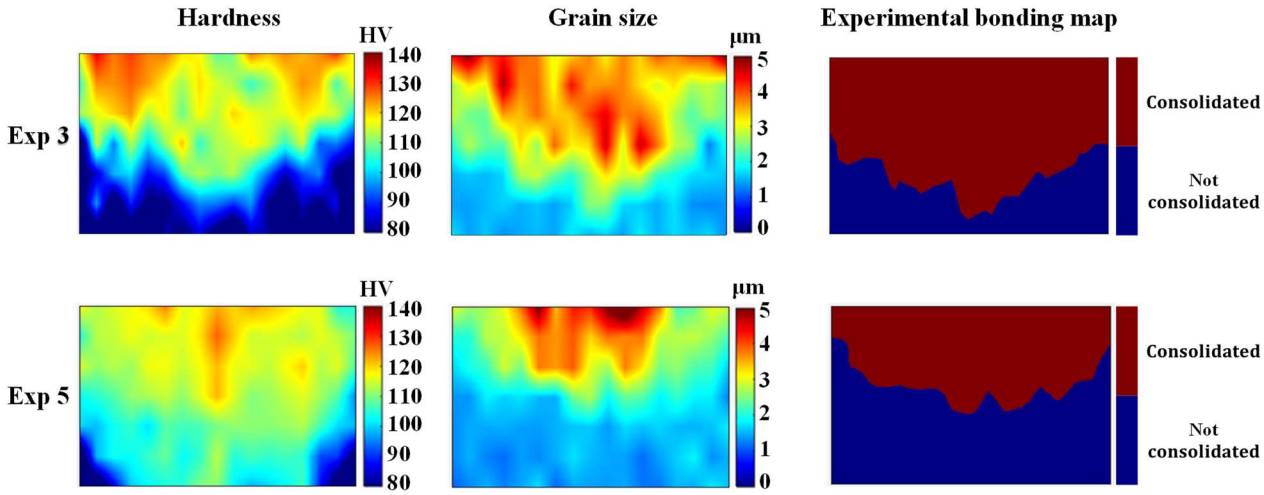

Fig. 17. Hardness, grain size and experimental bonding map for Exp 3 and Exp 5.

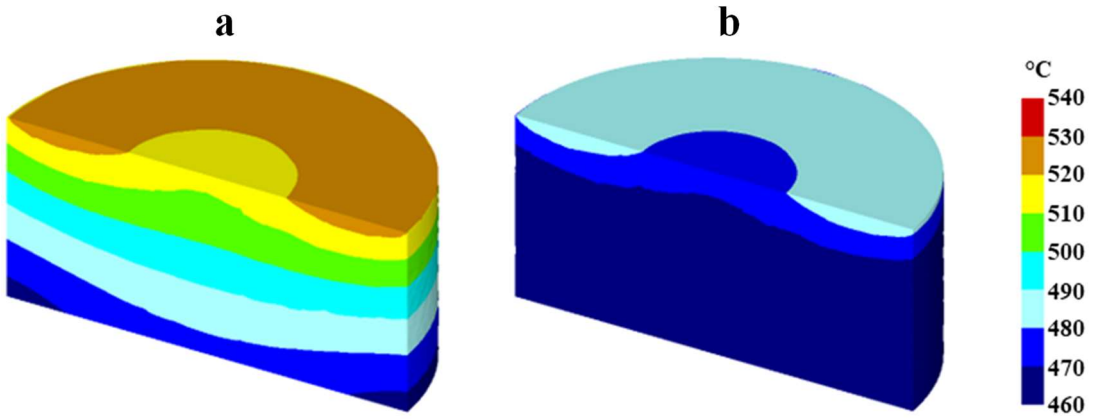

Fig. 18. Temperature distribution obtained from DEFORM 3D for (a) Exp 3 and (b) Exp 5.

The effects of different process parameters on the solid bonding phenomenon are also visible in the microstructure analysis reported in Fig. 19. The different process parameters lead to different defects occurrence, Exp 3 is characterized by better solid bonding consolidation and grain size refinement especially in the middle-side part of the billet, moreover in Exp 5 more evident defects are visible in the bottom region of the billet. A similar trend was observed while discussing the effect of rotational speed in section 3.1 (Fig. 8).

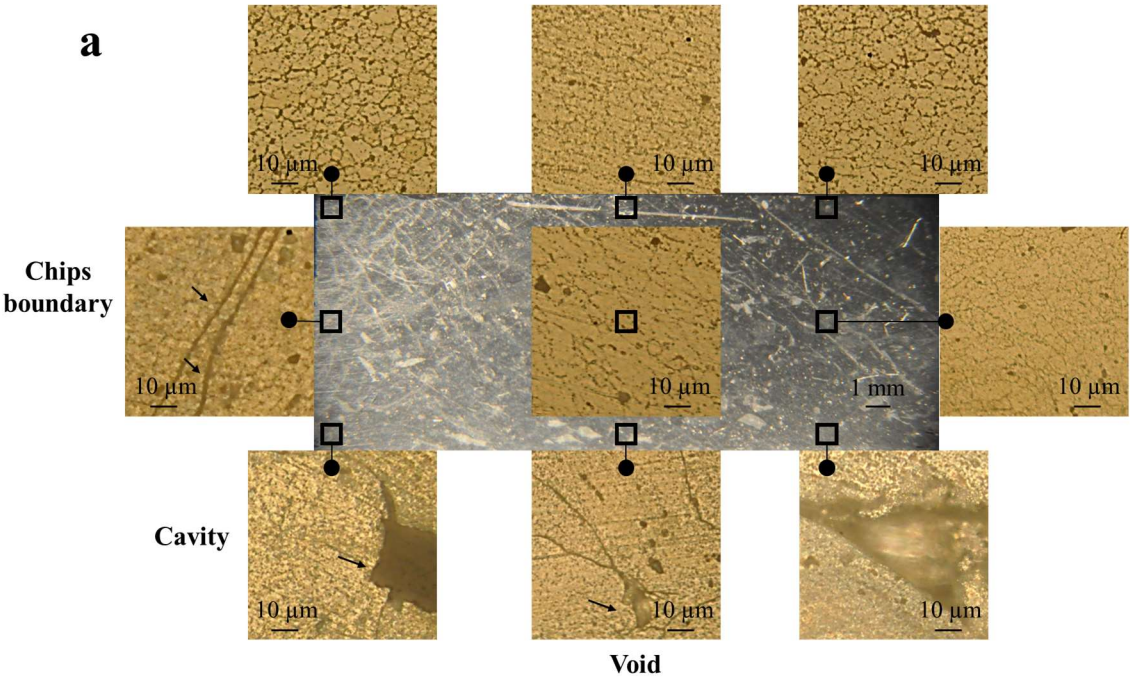

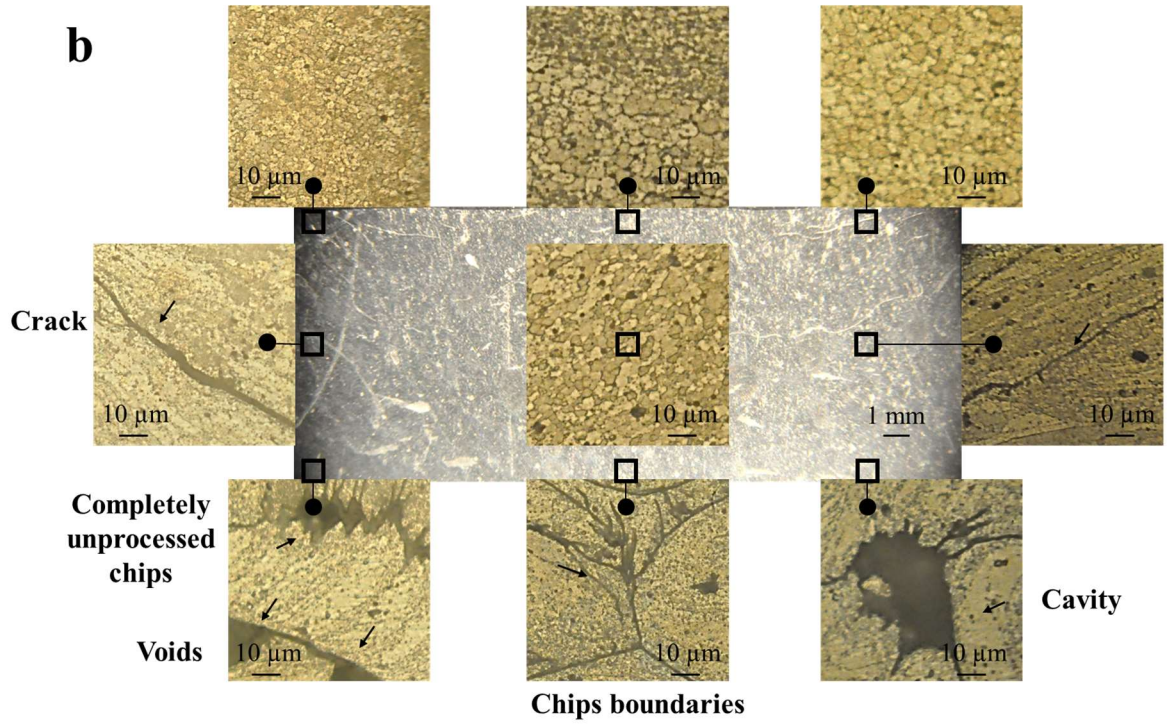

Fig. 19. Microstructure of AA70775 FSC billet section for (a) Exp 3 and (b) Exp 5

Overall, the aim is to turn all the experimental and numerical knowledge, acquired by developing experiments from Exp 1 to 4, into a model able to predict the solid bonding occurrence during friction stir consolidation process of AA7075 alloy. For a correct model implementation, a validation procedure is needed; in the present paper the testing procedure for each criterion was implemented by the following workflow.

1. Interpolating, by third order polynomial fitting curve, the W_{Ci}^{lim} reported in Fig. 15.
2. Formulating analytical expressions able to link the W_{Ci}^{lim} with temperature.
3. Performing the FSC for Exp 5 and 6 of Table 2.
4. Measuring the hardness and the grain size of Exp 5 and 6 (for the 119 loci).
5. Performing the numerical simulation and extracting temperature, strain and stress variables.
6. Calculating the different Wi (i = 1 to 119) values for the 119 loci.
7. Calculating for each loci the W_{Ci}^{lim} (i = 1 to 119) with the model developed in step 2.
8. Predicting for each loci the bonding/non-bonding occurrence (if Wi $\geq$ $W_{Ci}^{lim}$the point is labelled as fully consolidated, elsewhere it is considered non-consolidated).
9. Comparing the predicted values with the experimental results.
10. Quantifying the prediction accuracy of each analyzed criterion.

The results of the testing procedure are reported in tables 5 and 6 for Exp 5 and 6, respectively. It is possible to see that the best performance in predicting the bonding occurrence in FSC are provided by the C5. In fact, a prediction error, number of loci mistakenly predicted divided by the total number of tested loci, equal to 6 % for Exp 5 and 10 % for Exp 6 was observed. Good performance is provided also by C3 criterion although the error for Exp 6 rises up to 21%. All the other criteria are not eligible as the prediction error performances are not satisfactory in both of the analyzed experiments.

Table 5 Bonding criteria prediction performance for Exp 5.

Criterion	N° loci correctly predicted	N° total loci	Prediction error [%]
C1 - Akeret	70	119	42
C2 - Plata - Piwnik	79		34
C3 - Donati and Tomesani	108		10
C4 - Kolpak et al.	66		45
C5 - Plata – Piwnik - weighted	112		6
C6 - Plata - Piwnik - Zener	73		39

Table 6 Bonding criteria prediction performance for Exp 6.

Criterion	N° loci correctly predicted	N° total loci	Prediction error [%]
C1 - Akeret	60	119	50
C2 - Plata - Piwnik	53		56
C3 - Donati and Tomesani	95		21
C4 - Kolpak et al.	65		46
C5 - Plata – Piwnik - weighted	108		10
C6 - Plata - Piwnik - Zener	54		55

Fig. 20 provides a specific visualization of the experimental bonding map (Fig. 20a) for Exp 5 and the related predicted consolidated zone obtained using the C5 criterion (Fig. 20b). In this visualization, each analyzed point is modelled as a rectangle, in Fig. 20b the not correctly predicted loci are also highlighted. Overall, it is possible notice the predicted shape is very close to the experimental bonding area, and the prediction errors occur in the transition zone (region between the consolidated and not consolidated areas). In this area, the hardness and grain size values are close to the threshold values, also, it may occur that either the hardness or the grain size values exceed the value of the thresholds previously identified. This area is very close to the bonding conditions making the prediction very challenging to be implemented.

In order to highlight the improvement obtained with the here proposed Plata – Piwnik - weighted (C5) criterion a comparison with a standard one is reported. Specifically, the predicted bonding map for Exp 5 using the Plata – Piwnik criterion (C2) is reported in Fig. 20c. As it is possible to notice the bonding area is significantly different from the experimental one, in particular an overestimation of the bonding occurrence is predicted. It is worth remarking that the same trends were also observed while analyzing the prediction of the criteria for Exp 6.

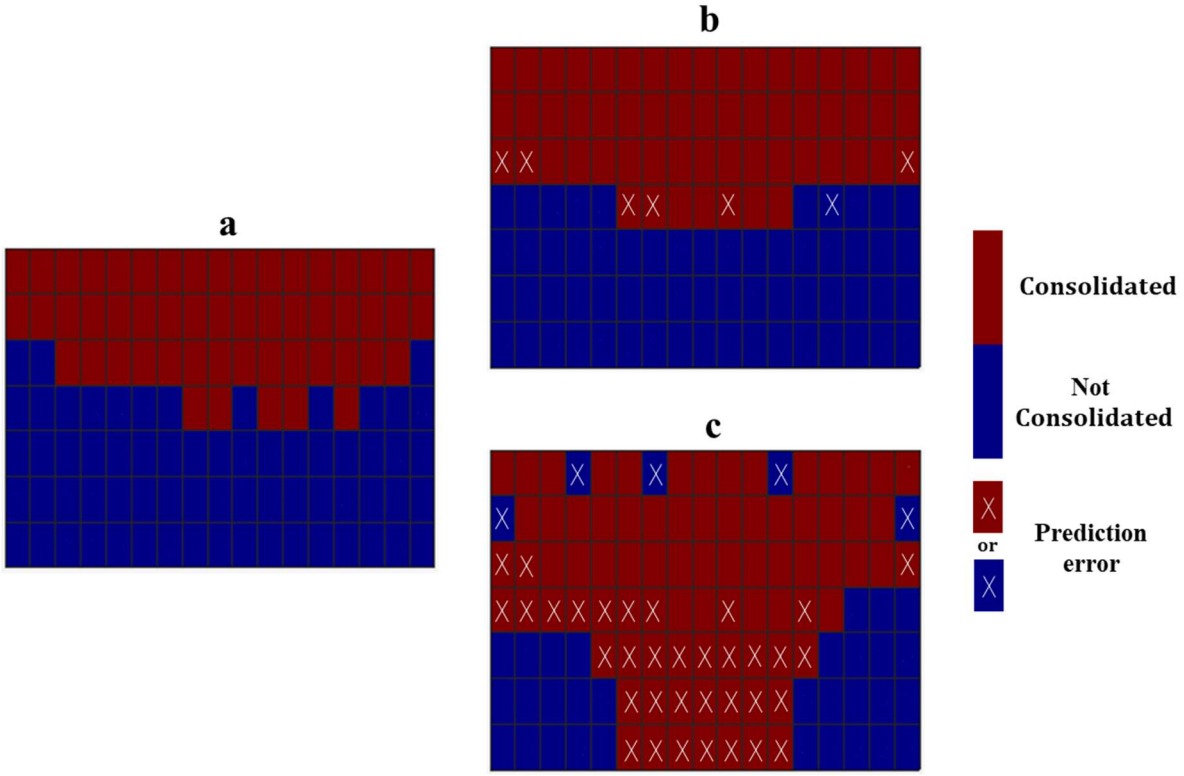

Fig. 20. (a) Experimental bonding map for Exp 5, (b) predicted boning area of Plata – Piwnik - weighted (C5) criterion prediction and (c) Plata – Piwnik (C2) criterion prediction.

It is worth remarking that the proposed criterion, beyond being the only capable of modelling the bonding condition for FSC, is also characterized by a relatively low level of complexity if compared to the approaches based on the film theory (Kolpak et al 2019). Actually, for the implementation of the Plata-Piwnik weighed criterion the decisive factor is just the identification of the bonding limit with varying the temperature, the same requirement is essential also for Plata-Piwnik (Ceretti et al, 2009)

5. Conclusions

In this paper different solid bonding criteria have been tested for the modelling of chips recycling by Friction Stir Consolidation. The performances of conventional criteria have been compared with that of a new, here proposed, bonding criterion. The analyses were performed by setting up a procedure for the automatic evaluation of the threshold values of the different analyzed bonding criteria.

The developed analyses allow to draw some main findings.

1/ Conventional bonding criteria already available in literature fail to predict the solid bonding occurrence for FSC recycling.

2/ The failure is mainly due to the peculiar nature of FSC process: strain and strain rate values are limited (especially during the consolidation time) with minimum material flow within the die. This makes the criteria already tested for extrusion-based approaches ineffective.

3/ For all the analyzed criteria it was not possible to identify a unique W_{Ci}^{lim} value with varying process conditions and a temperature dependent model was identified for each criterion.

4/ A new and accurate analytical solid bonding criterion, named Plata – Piwnik – weighted criterion, specifically designed for FSC is proposed. The new criterion is characterized by three strengths: its trend decreases with increasing the temperature (and this is in line with what expected considering the physics of the process), provides a better prediction occurrence accuracy for a given processing time and is characterized by the best performances in the developed validation test. Concerning the latter aspect, two validation tests were performed varying the process parameters. Actually, a maximum prediction error equal to 10 % was observed, this score in significantly lower than those observed for the other criteria, for instance the conventional Plata – Piwnik criterion is characterized by an average prediction error equal to 45 % (almost half of the observation loci are incorrectly predicted).

Further development will concern the implementation of such procedure on different aluminum alloys and process variants in order to further test the flexibility of the proposed approach. The final aim would be the identification of a parametric model in order to describe, with a single analytical expression, the bonding occurrence of a cluster of different materials. Moreover, since the bonding occurrence of FSC is due to the effect of different variables, a machine learning based prediction approach will be implemented. The aim of machine learning implementation would be both the identification of other significant variables and a further improvement of the solid boning occurrence prediction performance.

Acknowledgments

This study was carried out within the MICS (Made in Italy – Circular and Sustainable) Extended Partnership and received funding from the European Union Next-Generation EU (PIANO NAZIONALE DI RIPRESA E RESILIENZA (PNRR) – MISSIONE 4 COMPONENTE 2, INVESTIMENTO 1.3 – D.D. 1551.11-10-2022, PE00000004). This manuscript reflects only the authors' views and opinions, neither the European Union nor the European Commission can be considered responsible for them.

References

Akeret, R., 1992. Extrusion welds-quality aspects are now center stage. Proceedings of the 5th International Aluminum Extrusion Technology Seminar, vol. 1, 319–336.

Allwood, J. M., Cullen, J. M., 2012. Sustainable materials: with both eyes open (Vol. 2012). Cambridge, UK: UIT Cambridge Limited.

Ashby MF. The materials life cycle. In: Butterworth, Heinemann, editors. Materials and the Environment: ELSEVIER; 2021,41-64.

Baffari, D., Buffa, G., Fratini, L., 2017. A numerical model for Wire integrity prediction in Friction Stir Extrusion of magnesium alloys. Journal of Materials Processing Technology, 247, 1-10.

Bay, N. 1979. Cold pressure welding—the mechanisms governing bonding.

Behrens, B. A., Frischkorn, C., & Bonhage, M. 2014. Reprocessing of AW2007, AW6082 and AW7075 aluminium chips by using sintering and forging operations. *Production Engineering*, *8*, 443-451.

Buffa, G., Hua, J., Shivpuri, R., & Fratini, L. 2006. A continuum based fem model for friction stir welding—model development. *Materials Science and Engineering: A*, *419*(1-2), 389-396.

Buffa, G., Pellegrino, S., Fratini, L., 2014. Analytical bonding criteria for joint integrity prediction in friction stir welding of aluminum alloys. Journal of Materials Processing Technology, 214(10), 2102-2111.

Ceretti, E., Fratini, L., Gagliardi, F., Giardini, C., 2009. A new approach to study material bonding in extrusion porthole dies. CIRP annals, 58(1), 259-262.

Chiba, R., Nakamura, T., Kuroda, M., 2011. Solid-state recycling of aluminium alloy swarf through cold profile extrusion and cold rolling. Journal of Materials Processing Technology, 211(11), 1878-1887.

Chiba, R., Yoshimura, M. 2015. Solid-state recycling of aluminium alloy swarf into c-channel by hot extrusion. Journal of Manufacturing Processes, 17, 1-8.

Cislo, C. N., Kronthaler, B., Buchmayr, B., & Weiß, C. 2020. Solid state recycling of aluminum alloy chips via pulsed electric current sintering. *Journal of Manufacturing and Materials Processing*, *4*(1), 23.

Cooper, D.R., Allwood, J.M., 2014. The influence of deformation conditions in solid-state aluminium welding processes on the resulting weld strength. J. Mater. Process. Technol. 214, 2576–2592.

Donati, L., Tomesani, L., 2004. The prediction of seam welds quality in aluminum extrusion. J. Mater. Process. Technol. 153-154, 366–373.

Duflou, J.R., Tekkaya, A. E., Haase, M., Welo, T., Vanmeensel, K., Kellens, K., Dewulf, W., Paraskevas, D. (2015). Environmental assessment of solid state recycling routes for aluminium alloys: can solid state processes significantly reduce the environmental impact of aluminium recycling?. Cirp Annals, 64(1), 37-40.

Güley, V., Güzel, A., Jäger, A., Ben Khalifa, N., Tekkaya, A.E., Misiolek, W.Z., 2013. Effect of die design on the welding quality during solid state recycling of AA6060 chips by hot extrusion. Mater. Sci. Eng. 574, 163–175.

Haase, M., Khalifa, N.B., Tekkaya, A.E., Misiolek, W. Z., 2012. Improving mechanical properties of chip-based aluminum extrudates by integrated extrusion and equal channel angular pressing (iECAP). Mat Sci Eng A 2012; 539: 194-204. https://doi.org/10.1016/j.msea.2012.01.081.

Haase, M., Tekkaya, A.E., 2015. Cold extrusion of hot extruded aluminum chips. Journal of Materials Processing Technology, 217, 356-367.

International Energy Agency. https://www.iea.org/ [accessed May 2023].

Koch, A., Bonhage, M., Teschke, M., Luecker, L., Behrens, B. A., & Walther, F., 2020. Electrical resistance-based fatigue assessment and capability prediction of extrudates from recycled field-assisted sintered EN AW-6082 aluminium chips. *Materials Characterization*, *169*, 110644.

Kolpak, F., Schulze, A., Dahnke, C., Tekkaya, A.E., 2019. Predicting weld-quality in direct hot extrusion of aluminium chips. Journal of Materials Processing Technology, 274, 116294.

Latif, A., Ingarao, G., Gucciardi, M., Fratini, L., 2022. A novel approach to enhance mechanical properties during recycling of aluminum alloy scrap through friction stir consolidation. The International Journal of Advanced Manufacturing Technology, 119(3-4), 1989-2005.

Latif A., Ingarao, G., Fratini, L., 2022. Multi-material based functionally graded billets manufacturing through friction stir consolidation of aluminium alloys chips. CIRP Annals, 71(1), 261-264.

Latif, A., Ingarao, G., Fratini, L., Hetz, P., & Merklein, M., 2023. Characterization of friction stir consolidated recycled billet by uniaxial compression tests with miniaturized cylindrical specimen. *materials research proceedings*, *28*, 1997-2004.

Li, B., Teng, B., & Zhu, Z., 2020. Solid state recycling of Mg–Gd–Y–Zn–Zr alloy chips by spark plasma sintering. *Journal of Magnesium and Alloys*, *8*(4), 1154-1165.

Li, X., Baffari, D., Reynolds, A. P.,2018. Friction stir consolidation of aluminum machining chips. The International Journal of Advanced Manufacturing Technology, 94, 2031-2042.

Lui, E.W., Palanisamy, S., Dargusch, M.S., Xia, K., 2016. Effects of chip conditions on the solid state recycling of Ti-6Al-4V machining chips. Journal of Materials Processing Technology, 238, 297-304.

Overman, N.R., Olszta, M. J., Bowden, M., Li, X., Rohatgi, A., Mathaudhu, S.N., Whalen, S. A., 2021. The onset of alloying in Cu-Ni powders under high-shear consolidation. Materials Design, 211, 110151.

Paraskevas, D., Dadbakhsh, S., Vleugels, J., Vanmeensel, K., Dewulf, W., & Duflou, J. R., 2016. Solid state recycling of pure Mg and AZ31 Mg machining chips via spark plasma sintering. *Materials & Design*, *109*, 520-529.

Paraskevas, D., Vanmeensel, K., Vleugels, J., Dewulf, W., Deng, Y., & Duflou, J. R., 2014. Spark plasma sintering as a solid-state recycling technique: the case of aluminum alloy scrap consolidation. *Materials*, *7*(8), 5664-5687.

Pei, Y., Ma, H., Yuan, M., & Teng, B., 2022. Solid state recycling of Mg–Gd–Y–Zn–Zr alloy chips by isothermal sintering and equal channel angular pressing. *Journal of Magnesium and Alloys*.

Plata, M., Piwnik, J., 2000. Theoretical and experimental analysis of seam weld formation in hot extrusion of aluminium alloys. Proceedings of the 7th International Aluminium Extrusion Seminar 205–212.

Rofman, O. V., Prosviryakov, A.S., Mikhaylovskaya, A.V., Kotov, A.D., Bazlov, A.I., Cheverikin, V. V., 2019. Processing and microstructural characterization of metallic powders produced from chips of AA2024 alloy. JOM, 71, 2986-2995.

Shima S, Oyane M., 1976. Plasticity theory for porous metals. International Journal of Mechanical Sciences;18:285–91. doi:10.1016/0020-7403(76)90030-8.

Tang, W., Reynolds, A.P., 2010. Production of wire via friction extrusion of aluminum alloy machining chips. Journal of Materials Processing Technology, 210(15), 2231-2237.

Tang, W., Reynolds, A.P., 2011. Friction consolidation of aluminum chips TMS Annual Meeting, pp. 289-298. Cited 4 times. https://www.tms.org/ISBN: 978-111800201-8. doi: 10.1002/9781118062302.ch34.

Tekkaya, A.E., Schikorra, M., Becker, D., Biermann, D., Hammer, N., Pantke, K., 2009. Hot profile extrusion of AA-6060 aluminum chips. Journal of materials processing technology, 209(7), 3343-3350.

Tolio, T., Bernard, A., Colledani, M., Kara, S., Seliger, G., Duflou, J., Battaia, O., Takata, S.,2017. Design, management and control of demanufacturing and remanufacturing systems. CIRP Annals, 66(2), 585-609.

Whalen, S., Taysom, B.S., Overman, N., Reza-E-Rabby, M., Qiao, Y., Richter, T., Skszek, T., DiCiano, M., 2023. Porthole die extrusion of aluminum 6063 industrial scrap by shear assisted processing and extrusion. Manufacturing Letters, 36, 52-56.

Widerøe, F., & Welo, T., 2013. Using contrast material techniques to determine metal flow in screw extrusion of aluminium. Journal of Materials Processing Technology, 213(7), 1007-1018.